Atmos. Meas. Tech. Discuss., 7, 633–701, 2014
www.atmos-meas-tech-discuss.net/7/633/2014/
doi:10.5194/amtd-7-633-2014

Atmospheric Measurement Techniques Discussions

Tropospheric CH_4 signals as observed by NDACC FTIR at globally distributed sites and comparison to GAW surface in-situ measurements

E. Sepúlveda[1,2], M. Schneider[3], F. Hase[3], S. Barthlott[3], D. Dubravica[3], O. E. García[1], A. Gomez-Pelaez[1], Y. González[1], J. C. Guerra[2], M. Gisi[3,*], R. Kohlhepp[3,], S. Dohe[3], T. Blumenstock[3], K. Strong[4], D. Weaver[4], M. Palm[5], A. Sadeghi[5], N. M. Deutscher[5,6], T. Warneke[5], J. Notholt[5], N. Jones[6], D. W. T. Griffith[6], D. Smale[7], G. W. Brailsford[7], J. Robinson[7], F. Meinhardt[8], M. Steinbacher[9], T. Aalto[10], and D. Worthy[11]**

[1]Izaña Atmospheric Research Center, Agencia Estatal de Meteorología (AEMET), Tenerife, Spain
[2]Department of Physics, University of La Laguna (ULL), Tenerife, Spain
[3]Institute for Meteorology and Climate Research, Karlsruhe Institute of Technology (KIT), Karlsruhe, Germany
[4]Department of Physics, University of Toronto (UofT), Toronto, Canada
[5]Institute of Environmental Physics, University of Bremen (UB), Bremen, Germany

[6]Centre for Atmospheric Chemistry, University of Wollongong (UOW), Wollongong, Australia
[7]National Institute of Water and Atmospheric Research (NIWA), Lauder, New Zealand
[8]Federal Environmental Agency Germany (UBA), Dessau-Roßlau, Germany
[9]Swiss Federal Laboratories for Materials Science and Technology (EMPA), Dübendorf, Switzerland
[10]Climate Change Research, Finnish Meteorological Institute (FMI), Helsinki, Finland
[11]Climate Research Division, Environment Canada (EC), Wellington, Canada
[*]now at: Bruker Optics GmbH, Ettlingen, Germany
[**]now at: Deutscher Wetterdienst, Offenbach, Germany

Received: 24 December 2013 – Accepted: 12 January 2014 – Published: 27 January 2014

Correspondence to: E. Sepúlveda (elisepul@ull.es)

Published by Copernicus Publications on behalf of the European Geosciences Union.

AMTD
7, 633–701, 2014

Abstract

We present lower/middle tropospheric column-averaged CH_4 mole fraction time series measured by nine globally distributed ground-based FTIR (Fourier Transform InfraRed) remote sensing experiments of the Network for the Detection of Atmospheric Composition Change (NDACC). We show that these data are well representative of the tropospheric regional-scale CH_4 signal, largely independent of the local small-scale signals of the boundary layer, and only weakly dependent on upper tropospheric/lower stratospheric (UTLS) CH_4 variations. In order to achieve the weak dependency on the UTLS, we use an a posteriori correction method. We estimate a typical precision for daily mean values of about 0.5 % and a systematic error of about 2.5 %. The theoretical assessments are complemented by an extensive empirical study. For this purpose, we use surface in-situ CH_4 measurements made within the Global Atmosphere Watch (GAW) network and compare them to the remote sensing data. We briefly discuss different filter methods for removing the local small-scale signals from the surface in-situ datasets in order to obtain the in-situ regional-scale signals. We find good agreement between the filtered in-situ and the remote sensing data. The agreement is consistent for a variety of time scales that are interesting for CH_4 source/sink research: day-to-day, monthly, and inter-annual. The comparison study confirms our theoretical estimations and proves that the NDACC FTIR measurements can provide valuable data for investigating the cycle of CH_4.

1 Introduction

Methane (CH_4) plays an important role in atmospheric chemistry, affecting the oxidizing capacity of the atmosphere, acting as a precursor of tropospheric ozone (O_3) and being the most important anthropogenic greenhouse gas after carbon dioxide (CO_2).

For many years, tropospheric greenhouse gases have been monitored at the Earth's surface by very precise in-situ techniques. However, surface measurements can be

AMTD
7, 633–701, 2014

strongly affected by local small-scale processes, and by this reason surface GAW stations have been located in very particular places where there is no influence of small-scale process at least part of the time in order to get regional representative measurements (especially for Global GAW stations).

Observations above the boundary layer are well representative of the lower tropospheric regional-scale evolution of CH_4 and thus they could well complement the surface in-situ datasets. For instance, Olsen and Randerson (2004) proposed using total column-averaged observations of CO_2 as valid input for inverse models. For CH_4, however, the strong vertical gradient in the stratosphere has a significant effect on the column averages. The CH_4 column average is therefore strongly dependent on the tropopause altitude, which means, for instance, that the seasonal cycle in column-averaged CH_4 can significantly differ from that in the free troposphere (e.g. Sepúlveda et al., 2012). The uncertainty in modeling the variations of the tropopause altitude and of stratospheric CH_4 significantly limits the usefulness of total column-averaged CH_4 observations for inverse modeling purposes.

Figure 1 gives an overview of the different atmospheric CH_4 signals. The grey bar indicates the very high and very local typical small-scale variability that might occur within the first few hundred meters above the surface. This signal is caused by local sources and sinks. In the upper troposphere/lower stratosphere (UTLS), the CH_4 mole fraction depend on the tropopause altitude. The blue area indicates the variability due to a ±100 hPa variability of the tropopause (e.g. Hoinka, 1998). This signal is mainly uniform over the whole UTLS, i.e. a tropopause shift causes strongly correlated variations from the tropopause up to the middle stratosphere.

The red area represents the typical variability in the free troposphere of about 2 %. Although the troposphere is typically well-mixed, the chemical activity of CH_4 (e.g. destruction by OH) can cause differences between lower/middle and upper tropospheric CH_4 mole fraction, and the vertical correlation of the tropospheric CH_4 variability is very likely limited to about 5–10 km. This tropospheric variability (or even better its lower tropospheric portion) would be a very suitable inverse model input. However, its

AMTD
7, 633–701, 2014

measurements by remote sensing techniques are difficult since this tropospheric signal is much smaller than the boundary layer or the UTLS signal.

Previous studies have shown tropospheric CH_4 mole fraction obtained by middle-infrared FTIR and in-situ techniques, e.g. Rinsland et al. (2005). Sepúlveda et al. (2012) documented theoretically and empirically that the ground-based FTIR experiments operated within the NDACC (Network for the Detection of Atmospheric Composition Change, http://www.acd.ucar.edu/irwg/, Kurylo and Zander, 2000) can provide some information on the vertical distribution of atmospheric CH_4. They empirically documented the quality of these profile data: first, for the lower tropospheric FTIR CH_4 data there is good agreement with coincident free tropospheric GAW in-situ observations and second, for the UTLS the FTIR measures CH_4 mole fraction that shows a strong anti-correlation with the stratospheric proxy HF. The profiling capability is not only important for CH_4 source/sink research applications, it is also an advantage when validating column-averaged CH_4 obtained from satellites, since it allows the vertical sensitivity of the satellite data to be accounted for. In this paper, we extend the Sepúlveda et al. (2012) study, which is limited to a subtropical site, to a set of nine globally-distributed NDACC FTIR stations covering polar, mid-latitudinal, and subtropical regions and we focus on the quality of the lower free tropospheric CH_4 FTIR data. We document that the data are largely independent of the local small-scale signals of the boundary layer, and only weakly dependent on upper tropospheric/lower stratospheric (UTLS) CH_4 variations. Furthermore, we find a reasonable consistency for the different NDACC FTIR sites.

This manuscript is organized as follows: Sect. 2 explains the ground-based NDACC FTIR technique, the CH_4 retrieval strategy, and an overview of the NDACC sites involved in this study. Section 3 discusses the different NDACC remote sensing and GAW in-situ datasets used in this work. Section 4 shows the comparison between the NDACC and GAW data and Sect. 5 provides a summary and conclusion.

AMTD
7, 633–701, 2014

2 Ground-based NDACC FTIR: experiment, tropospheric CH_4 retrieval setup, and error estimation

In this section we briefly describe the ground-based FTIR measurements performed within NDACC, the retrieval setup we have used for our study, the theoretical error analysis, and the locations of the participating stations.

2.1 NDACC FTIR experiments

NDACC is a global network community that monitors changes in atmospheric composition. It provides long-term observations of many trace gases and allows assessment of their impact on global climate. It is composed of more than 70 high-quality remote-sensing research stations operating several different measurement techniques. Currently, 22 NDACC sites operate with ground-based FTIR spectrometers. This study applies data obtained with the FTIR technique. The commercial Bruker IFS 125HR is one of the most modern FTIR instruments used in the network. Also the older version 120HR and the portable version 120M with slightly worse signal-to-noise ratio and less favourable instrumental line shape (ILS) characteristics and temporal stability are still in use.

The NDACC FTIR instrumentation consists of a high quality FTIR spectrometer and a high precision solar tracker controlled by a combination of astronomical calculations and a solar quadrant or more recently a digital camera (Gisi et al., 2011) for active tracker control. The experiments record direct solar spectra in the middle-infrared spectral region (740–4250 cm^{-1}, corresponding to 13.5–2.4 µm), with a resolution of 0.0035–0.005 cm^{-1} and work under clear sky conditions. This implies that the line of sight must be free of clouds and during night no measurements are possible. However, measurements with less sensitivity using the moon as the light source have been reported (Notholt et al., 1993; Notholt and Lehmann, 2003; Wood et al., 2004) but are not used in this study.

AMTD
7, 633–701, 2014

These high quality solar absorption spectra have been measured over many years and at many different sites (the first measurements started in the early nineties when the network was named the Network for the Detection of Stratospheric Change, NDSC). The measurements disclose significant information about the distribution of many different atmospheric trace gases. During recent years, the NDACC FTIR community has increased its efforts to monitor tropospheric mole fraction, including water vapour (Schneider et al., 2006a, b), and methane (e.g. Sussmann et al., 2012; Sepúlveda et al., 2012).

The ground-based NDACC FTIR stations involved in this study are nine globally distributed sites between the Arctic and the Antarctic. All of these stations contribute to the MUSICA project (MUlti-platform remote Sensing of Isotopologues for investigating the Cycle of Atmospheric water, Schneider et al., 2012). The stations are listed in Table 1 and site locations displayed in Fig. 2. The spectra for each station have been analysed in a uniform way, thereby ensuring good consistency of the ground-based CH_4 remote sensing data.

NDACC FTIR data are generally available on the NDACC database (http://www.ndsc.ncep.noaa.gov/data/). The CH_4 product presented here is not yet publicly available, however, we plan to make it available as part of the MUSICA project data that are currently published on the NDACC database in the project data section.

2.2 The tropospheric CH_4 profile retrieval setup

The measured spectra are analysed with the inversion code PROFFIT (PROFile FIT, Hase et al., 2004), which has been applied for many years by a part of the ground-based FTIR community for evaluating high resolution solar absorption spectra. The code simulates the spectra and the Jacobians by the line-by-line radiative transfer model PRFFWD (PRoFit ForWarD model, Hase et al., 2004; Schneider and Hase, 2009). It includes a ray tracing module (Hase and Höpfner, 1999) in order to precisely simulate how the radiation passes through the atmosphere.

AMTD
7, 633–701, 2014

The vertical structure of the atmosphere is discretised and the amount of the absorber x at altitude level z can be described in form of a vector $\boldsymbol{x}(z)$. Similarly the radiation spectrum is discretised and described by a vector $\boldsymbol{y}$ containing the radiances at the different spectral bins. PRFFWD accounts for the forward relation (**F**), that connects the spectrum ($\boldsymbol{y}$) to the vertical distribution of the absorbers ($\boldsymbol{x}$) and to parameters ($\boldsymbol{p}$) describing the state of the atmosphere and instrumental characteristics:

$$\boldsymbol{y} = \mathbf{F}(\boldsymbol{x}, \boldsymbol{p}) \tag{1}$$

The retrieval adjusts the amount of the absorbers to obtain a best fit between the measured and simulated spectra. This is an under-determined problem, i.e. there are many different atmospheric states ($\boldsymbol{x}$) that produce almost identical spectra ($\boldsymbol{y}$). Consequently the problem requires some kind of constraint or regularisation. PROFFIT introduces the regularisation by means of a cost function:

$$[\boldsymbol{y} - \mathbf{F}(\boldsymbol{x}, \boldsymbol{p})]^{\mathrm{T}} \mathbf{S}_{\epsilon}^{-1} [\boldsymbol{y} - \mathbf{F}(\boldsymbol{x}, \boldsymbol{p})] + [\boldsymbol{x} - \boldsymbol{x}_{\mathrm{a}}]^{\mathrm{T}} \mathbf{S}_{\mathrm{a}}^{-1} [\boldsymbol{x} - \boldsymbol{x}_{\mathrm{a}}] \tag{2}$$

Here the first term is a measure for the difference between the measured spectrum ($\boldsymbol{y}$) and the spectrum simulated for a given atmospheric state ($\boldsymbol{x}$), whereby the actual measurement noise level is considered ($\mathbf{S}_{\epsilon}$ is the noise covariance). The second term is the regularisation term. It constrains the atmospheric solution state ($\boldsymbol{x}$) towards an apriori state ($\boldsymbol{x}_{\mathrm{a}}$), whereby the kind and the strength of the constraint are defined by the matrix ($\mathbf{S}_{\mathrm{a}}$). The constrained solution is reached at the minimum of the cost function Eq. (2).

Since the equations involved in atmospheric radiative transfer are non-linear, the cost function, Eq. (2), is minimised iteratively by a Gauss–Newton method. The solution for the $(i+1)$th iteration is:

$$\boldsymbol{x}_{i+1} = \boldsymbol{x}_{\mathrm{a}} + \mathbf{S}_{\mathrm{a}} \mathbf{K}_i^{\mathrm{T}} (\mathbf{K}_i \mathbf{S}_{\mathrm{a}} \mathbf{K}_i^{\mathrm{T}} + \mathbf{S}_{\epsilon})^{-1} [\boldsymbol{y} - \mathbf{F}(\boldsymbol{x}_i) + \mathbf{K}_i (\boldsymbol{x}_i - \boldsymbol{x}_{\mathrm{a}})] \tag{3}$$

where **K** is the Jacobian matrix which samples the derivatives $\partial \hat{x} / \partial y$ (changes in the spectral fluxes y for changes in the vertical distribution of the absorber x). These

AMTD
7, 633–701, 2014

regularisation and iteration methods are standard in the field of remote sensing. An extensive treatment of this topic is given in the textbook of Rodgers (2000).

Our CH_4 retrieval strategy is essentially the one described in Sepúlveda et al. (2012), where we have presented CH_4 profile retrievals for the relatively dry high mountain site of Izaña. For this study we slightly change our microwindow selection in order to further reduce the impact of H_2O interferences, which might play a role for humid low-altitude sites. The chosen spectral microwindows are shown in Fig. 3. The new set of microwindows contains strong, not saturated, and well-isolated CH_4 absorption lines as well as H_2O and HDO lines, in order to better account for the H_2O and HDO interferences. Together with the spectral CH_4 signatures we consider H_2O, HDO, CO_2, O_3, N_2O, NO_2, HCl, and OCS signatures. We apply the HITRAN 2008 spectroscopy (with 2009 updates, Rothman et al., 2009), except for the target species CH_4, where we use line parameters obtained as a result of a current project of the Deutsche Forschungsgemeinschaft. IUP-Bremen, DLR-Oberpfaffenhofen, and KIT are involved in this activity. A preliminary linelist has been provided by D. Dubravica and F. Hase, KIT in December 2012 (see also, Dubravica et al., 2013) and it shows lower spectroscopic residuals than the HITRAN 2008 linelist.

The apriori knowledge for the interfering species are taken from the Whole Atmosphere Community Climate Model (WACCM version 5, provided by NCAR: National Centre for Atmospheric Research, J. Hannigan, personal communication, 2009). It is important to remark that we use station specific apriori data, but do not vary this apriori depending on season. This ensures that at an individual station all variability seen in our profiles comes exclusively from the measurement. We perform the inversion of the CH_4 profiles on a logarithmic scale (Hase et al., 2004; Schneider et al., 2006a) applying a Tikhonov–Phillips ad hoc constraint, that constrains the vertical slope of the profile (we do not apply diagonal constraints). The H_2O and HDO interferences are considered by including dedicated spectral H_2O and HDO windows and retrieving H_2O and HDO profiles, whereby we constrain the HDO/H_2O ratio (e.g. Schneider et al., 2006b). In order to account for the NO_2 signatures we scale the WACCM NO_2 profile.

AMTD
7, 633–701, 2014

For the rest of the minor interfering species, we simply simulate the spectral signatures according to the WACCM mole fraction. As in Sepúlveda et al. (2012), we calculate the tropospheric column-averaged CH_4 mole fraction directly from the measured spectra. Therefore, we average the retrieved CH_4 mole fraction for the first six atmospheric model levels above the station (i.e. we average the values within a lower tropospheric layer with a thickness of typically 2.5 km).

We use the NCEP analysis (National Centers for Environmental Prediction) at 12:00 UT as the temperature and pressure input profiles. In order to account for variations in the spectral baseline, we apply a second order fit for the continuum background.

We would like to remark that we apply exactly the same retrieval setup for all the FTIR stations.

2.3 Theoretical error estimation

In this section we present a theoretical quality assessment for the tropospheric CH_4 product. We do this in detail taking the Kiruna station as an example and in the form of an overview for the other stations. The error analysis is made according to the analytic method suggested by Rodgers (2000), where the difference between the retrieved and the real state, $(\hat{x} - x)$ the error, is linearised about a mean profile x_a (the applied apriori profile), the estimated model parameters $\hat{p}$, and the measurement noise ϵ:

$$(\hat{x} - x) = (\hat{\mathbf{A}} - \mathbb{I})(x - x_a) + \hat{\mathbf{G}}\hat{\mathbf{K}}_p(p - \hat{p}) + \hat{\mathbf{G}}\epsilon \quad (4)$$

Here $\mathbb{I}$ is the identity matrix, $\hat{\mathbf{A}}$ is the averaging kernel matrix, $\hat{\mathbf{G}}$ the gain matrix ($\mathbf{G} = (\mathbf{K}^T\mathbf{S}_\epsilon^{-1}\mathbf{K} + \mathbf{S}_a^{-1})^{-1}\mathbf{K}^T\mathbf{S}_\epsilon^{-1}$), and $\hat{\mathbf{K}}_p$ a sensitivity matrix to input parameters (instrumental line shape, spectroscopic parameters, etc). The gain matrix $\hat{\mathbf{G}}$ samples the derivatives $\partial\hat{x}/\partial y$ (changes in the retrieved CH_4-state $\hat{x}$ for changes at the spectral bin y).

Equation (4) identifies the three classes of errors. These are: (a) errors due to the inherent finite vertical resolution and the limited sensitivity of the observing system (smoothing error), (b) errors due to uncertainties in the input parameters applied in

AMTD
7, 633–701, 2014

the inversion procedure, and (c) errors due to measurement noise (with an assumed Gaussian noise with $\sigma = \epsilon$).

2.3.1 Vertical resolution and sensitivity (smoothing error)

When contemplating remotely-sensed vertical distribution profiles one must consider the inherent vertical resolution and the limited sensitivity of these data. The left panel of Fig. 4 shows typical averaging kernels (row kernels in the logarithmic scale) for the retrieved CH_4 profiles at Kiruna. The kernels correspond to a measurement made on 4 July 2012, with OPDmax (maximal optical path difference) of 180 cm, at a solar elevation angle of 42.8°, and with 8.1 mm of precipitable water vapour. We chose this observation since it is not exclusively representative for polar conditions (e.g. low solar elevation, low precipitable water vapour), instead it can also serve as an example for mid-latitudinal and/or subtropical observations. Lower/middle tropospheric kernels are depicted as red lines and kernels at and above the UTLS (> 11.5 km) are depicted as blue lines. We observe that the FTIR measurements contain information about the vertical distribution from the surface up to the middle stratosphere. The trace (sum of diagonal elements) of the averaging kernel matrix is a measure of the degrees of freedom for signal (DOFS) in the measurement. It indicates the number of independent layers present in the retrieved profile (for the example shown in the left panel of Fig. 4 we have a DOFS of 2.6).

We see that the vertical resolution is about 8 km (Full-Width-Half-Maximum, FWHM, of the individual kernels). The tropospheric kernels (red lines) peak mainly in the troposphere and the stratospheric kernels (blue lines) mainly in the stratosphere. However, the plot also indicates contributions of the UTLS to the retrieved tropospheric CH_4 (negative values between 12 and 25 km for the red tropospheric kernels). This means that the stratospheric CH_4 variations might significantly affect the retrieved tropospheric CH_4 signals, especially since in the UTLS the typical CH_4 variation (caused by tropopause altitude shifts) is larger than the small tropospheric CH_4 variation.

AMTD
7, 633–701, 2014

For calculating the smoothing error we separate the signals into the three rather independent atmospheric CH_4 signals as described in Fig. 1: the small-scale boundary layer signal, the regional-scale tropospheric signal, and the UTLS signal. We assume (a) that there are very local small-scale variations of 20 % in a 100 m thick boundary layer (described by the apriori covariance matrix $\mathbf{S}_{a,bl}$), (b) that free tropospheric CH_4 typically varies with 2 % with correlation length of 5 km (apriori covariance $\mathbf{S}_{a,tro}$), and (c) that the altitude variation of the tropopause is typically about 100 hPa corresponding to a UTLS CH_4 variation of about 10–20 % and we use a correlation length of 10 km (apriori covariance $\mathbf{S}_{a,utls}$). For defining the typical CH_4 tropopause, we use the WACCM simulations. We define the tropopause altitude as the lowermost altitude where the CH_4 mole fraction are less than 95 % of the lower/middle free tropospheric CH_4 mole fraction (at 3 km altitude). This is typically 11 km for the polar, 13.5 km for the mid-latitudinal, and 18 km for subtropical sites, respectively.

The corresponding CH_4 smoothing error covariance matrices can be calculated by:

$$\mathbf{S}_{sm,bl} = \mathbf{A}\mathbf{S}_{a,bl}\mathbf{A}^T \quad (5)$$

$$\mathbf{S}_{sm,tro} = (\mathbf{A} - \mathbb{I})\mathbf{S}_{a,tro}(\mathbf{A} - \mathbb{I})^T \quad (6)$$

$$\mathbf{S}_{sm,utls} = \mathbf{A}\mathbf{S}_{a,utls}\mathbf{A}^T \quad (7)$$

Here $\mathbf{A}$ and $\mathbb{I}$ are the averaging kernel and the identity matrix, respectively.

The square root values of the diagonal elements of $\mathbf{S}_{sm,bl}$, $\mathbf{S}_{sm,tro}$, and $\mathbf{S}_{sm,utls}$ are depicted in the left panel of Fig. 5 as black, red, and green lines, respectively. The red line documents that the FTIR can well resolve the tropospheric background CH_4 signals (2 % variability, 5 km correlation length) with a precision of 0.4–1.2 % between the surface and 6 km altitude (for a 3 km thick layer the precision is 0.8 %). However, we have to consider cross dependency on the small-scale boundary layer variability and on the UTLS variability caused by shifts in the tropopause altitude. While the former adds an uncertainty of less than 0.2 % (black line), the latter has a large influence on the retrieved tropospheric CH_4 amounts (green line). In fact, the contribution from the

AMTD
7, 633–701, 2014

stratospheric CH_4 signal is clearly the leading smoothing error and adds an uncertainty of up to 1.5 % to the lower tropospheric CH_4 product.

2.3.2 Propagation of uncertainties

The assumed uncertainty sources are listed in Table 2. These values are critical to the error estimation. They come from our experience (e.g. repeatability of ILS, instrumental line shape, measurements) or from references (e.g. the spectroscopic parameter uncertainties are from Rothman et al., 2005). To minimise errors due to uncertainties of the instrumental line shape we monitor and eventually correct line shape distortions regularly every two months. These measurements consist of independent detections of cell absorption signatures as described in Hase et al. (1999). Baseline offsets might be produced by detector non-linearities. Similarly to other studies (Schneider and Hase, 2008) we assume the following uncertainties for instrumental parameters: measurement noise of 4 ‰, ILS (instrumental line shape, modulation efficiency and phase error) of 0.01 at OPDmax/10 and 0.1 rad, baseline offset of 1 ‰, baseline amplitude of 1 ‰, line of sight (solar tracker misalignment) of 0.1°. For uncertainties of the intensity and spectral position of solar lines we assume 1 % and 1×10^{-6} cm^{-1}, respectively. We separate the uncertainties of the atmospheric temperature into three components: the lower troposphere (< 5 km) with an uncertainty of 2 K, the upper troposphere (> 5 km) with an uncertainty of 2 K, and the stratosphere (> 15 km) with an uncertainty of 5 K. For the atmospheric H_2O and HDO profiles, which are obtained from the MUSICA retrieval, we assume an uncertainty of 10 % and 2 km uncertainty correlation length. Finally for the spectroscopic HITRAN intensity and pressure broadening parameters we use uncertainties of 2 % for all absorbers.

The error propagation of the different uncertainty sources as listed in Table 2 can be described by the error covariance ($\mathbf{S}_e$):

$$\mathbf{S}_e = \mathbf{G}\mathbf{K}_p\mathbf{S}_p\mathbf{K}_p^T\mathbf{G}^T \quad (8)$$

AMTD
7, 633–701, 2014

where **G** is the gain matrix, $\mathbf{K}_p$ is the parameter Jacobian, which samples the derivatives $\partial y/\partial p$ (changes at the spectral bin y for changes in the parameter p), and $\mathbf{S}_p$ is the uncertainty covariance matrix for parameter p.

The left panel of Fig. 6 depicts the square root of the diagonal elements of ($\mathbf{S}_e$). For this calculation, the partitioning between statistical and systematic error (fourth column in Table 2) is not considered, i.e. for assessing the error impact effect on the statistical or systematic error budget one has to scale these values accordingly. All of the propagated measurement noise error (black line, noi) and much of the propagated baseline error (red line, bas) are statistical errors, i.e. they dominate the statistical error budget. The systematic errors are dominated by uncertainties in the spectroscopic line parameters (dark cyan line, spe).

2.3.3 A posteriori correction for optimal independence of retrieved tropospheric and stratospheric CH_4

The left panel of Fig. 5 reveals that the retrieved tropospheric CH_4 amounts are strongly affected by cross dependencies on the stratospheric CH_4 signals. These cross-dependencies can be the leading error source. In this subsection we show that the cross dependencies can be significantly reduced by an a posteriori correction method. The method consists of a simple matrix multiplication and can be easily applied to any CH_4 profile retrieval whenever the retrieved CH_4 state is provided together with the corresponding averaging kernel.

The correction matrix (**C**) is constructed from entries of the averaging kernel matrix (**A**), which can be written as:

$$\mathbf{A} = \begin{pmatrix} \mathbf{A}_{TT} & \mathbf{A}_{ST} \\ \mathbf{A}_{TS} & \mathbf{A}_{SS} \end{pmatrix} \quad (9)$$

where $\mathbf{A}_{TT}$ describes how the tropospheric CH_4 signal affects the retrieved tropospheric amounts and $\mathbf{A}_{SS}$ how the stratospheric CH_4 affects the retrieved stratospheric

AMTD
7, 633–701, 2014

amounts. The cross-entries $\mathbf{A}_{ST}$ and $\mathbf{A}_{TS}$ describe the cross dependencies of the retrieved tropospheric amounts on the stratospheric signal and of the retrieved stratospheric amounts on the tropospheric signal, respectively. The $\mathbf{A}_{ST}$ cross-entries are responsible for the large smoothing error in the retrieved tropospheric CH_4 (green line in left panel of Fig. 5).

These cross-entries can be used for $\mathbf{C}$ as follows:

$$\mathbf{C} = \begin{pmatrix} \mathbb{I} & -\mathbf{A}_{ST} \\ -\mathbf{A}_{TS} & \mathbb{I} \end{pmatrix} \tag{10}$$

If we now modify $\mathbf{A}$ by multiplication with $\mathbf{C}$, we get the a posteriori corrected averaging kernel $\mathbf{A}^*$:

$$\begin{aligned} \mathbf{A}^* &= \mathbf{CA} \\ &= \begin{pmatrix} \mathbb{I} & -\mathbf{A}_{ST} \\ -\mathbf{A}_{TS} & \mathbb{I} \end{pmatrix} \begin{pmatrix} \mathbf{A}_{TT} & \mathbf{A}_{ST} \\ \mathbf{A}_{TS} & \mathbf{A}_{SS} \end{pmatrix} \\ &= \begin{pmatrix} \mathbf{A}_{TT} - \mathbf{A}_{ST}\mathbf{A}_{TS} & \mathbf{A}_{ST} - \mathbf{A}_{ST}\mathbf{A}_{SS} \\ -\mathbf{A}_{TS}\mathbf{A}_{TT} + \mathbf{A}_{TS} & -\mathbf{A}_{TS}\mathbf{A}_{ST} + \mathbf{A}_{SS} \end{pmatrix} \end{aligned} \tag{11}$$

Similarly we can modify the retrieved CH_4 state ($\hat{x}$) and calculate an a posteriori corrected CH_4 state $\hat{x}^*$:

$$\hat{x}^* = \mathbf{C}(\hat{x} - x_a) + x_a \tag{12}$$

The a posteriori corrected averaging kernels $\mathbf{A}^*$ (row kernels) are depicted in the central panel of Fig. 4. The blue kernels are for altitudes at and above 11.5 km and the green kernels are for the troposphere (for altitudes < 11.5 km). The right panel of Fig. 4 depicts the tropospheric surface row kernels of $\mathbf{A}^*$ together with the respective kernel of $\mathbf{A}$. The region of improvement is marked in the graph with a dashed circle. We see that for the a posteriori corrected row kernel (green line) there is much less cross talk

AMTD
7, 633–701, 2014

from the UTLS than for uncorrected/original kernel (red line). At the same, time the sensitivity with respect to the lower middle troposphere is not modified. It is apparent that the a posteriori correction allows for generation of a product that ensures an optimal separation between the retrieved tropospheric and stratospheric amounts.

The smoothing error covariance matrices for the corrected state can be calculated by:

$$\mathbf{S}^{*}_{\mathrm{sm,bl}} = \mathbf{CAS}_{\mathrm{a,bl}}\mathbf{CA}^{\mathrm{T}} \quad (13)$$

$$\mathbf{S}^{*}_{\mathrm{sm,tro}} = (\mathbf{CA} - \mathbb{I})\mathbf{S}_{\mathrm{a,tro}}(\mathbf{CA} - \mathbb{I})^{\mathrm{T}} \quad (14)$$

$$\mathbf{S}^{*}_{\mathrm{sm,utls}} = \mathbf{CAS}_{\mathrm{a,utls}}\mathbf{CA}^{\mathrm{T}} \quad (15)$$

For the corrected CH_4 state, the smoothing error caused by the stratospheric variability is significantly reduced in the troposphere if compared to the uncorrected state (compare green lines in the left and right panels of Fig. 5).

The error propagation for the a posteriori corrected state can be calculated by:

$$\mathbf{S}^{*}_{\mathrm{e}} = \mathbf{CGK}_{\mathrm{p}}\mathbf{S}_{\mathrm{p}}\mathbf{K}^{\mathrm{T}}_{\mathrm{p}}\mathbf{G}^{\mathrm{T}}\mathbf{C}^{\mathrm{T}} \quad (16)$$

The right panel of Fig. 6 shows the square root of the diagonal elements of $\mathbf{S}^{*}_{\mathrm{e}}$. We find that the a posteriori correction indeed only weakly affects the errors due to the parameter uncertainties of Table 2.

The a posteriori correction means an a posteriori optimisation of the retrieval constraints. The constraints are modified in order to get a tropospheric product that is optimally independent of the UTLS. A similar – although not equivalent – retrieval result might be achieved by already separating the tropospheric and stratospheric constraints in the original retrieval step. This has already been done, for instance, by Stiller et al. (1995), by means of a so-called "partitioning retrieval". The advantage of our a posteriori method is, that we get two products that are interesting: first, the optimally estimated profiles (no a posteriori correction), with good sensitivity from the lower troposphere up to the stratosphere, but with the UTLS cross talk on the tropospheric data. This is the

AMTD
7, 633–701, 2014

product that should be used for validating CH_4 total column measurements made by satellites. The second product is the optimally estimated tropospheric mole fraction. This product has slightly reduced sensitivity in the UTLS, where most satellites are sensitive, but it provides the best tropospheric CH_4 data quality and it is well-suited for tropospheric CH_4 source/sink research.

2.3.4 Error discussion

Table 3 summarizes the theoretical quality assessment of the CH_4 retrievals. The table lists DOFS values and the errors for the lower tropospheric column-averaged CH_4 product with and without applying the a posteriori correction as suggested in the previous subsection. The errors obtained if no a posteriori correction is applied are given in parenthesis.

At all stations, except Arrival Heights, we have typical DOFS close to or above 2.5. This means that we can estimate some details of the vertical distribution of the CH_4 mole fraction. However, we have to be aware that the lower tropospheric CH_4 signals (tropospheric CH_4 variations) are rather small compared to the UTLS signals (CH_4 variations due to variations of the tropopause altitude). This means that the small cross dependency of the retrieved lower tropospheric CH_4 mole fraction on the CH_4 state of the UTLS can significantly affect the quality of the lower tropospheric column-averaged CH_4 product. As a consequence, the UTLS smoothing error is a leading uncertainty source and dominates the overall smoothing errors in the lower troposphere (recall left panel of Fig. 5). This error is the more important, the lower the tropopause (it is more important for the polar than for the subtropical sites) and it can occasionally exceed 2 %, which is on the same order as the tropospheric CH_4 variations. In this context it is important to note that the UTLS smoothing error is actually not a purely random error. Since the tropopause altitude has a seasonal cycle this error will also depend on the season. It will mainly cancel out in the annual mean data but it will be responsible for major uncertainties in the lower tropospheric CH_4 seasonal cycles estimated from the FTIR observations. Therefore, if the objective is a precise tropospheric CH_4 product,

AMTD
7, 633–701, 2014

it is important to apply the a posteriori correction. The method reduces the cross talk for the stratosphere on the tropospheric CH_4 product at all sites, in particular at the polar regions (low tropopause altitude) where the cross dependency on the UTLS is particularly important. For the a posteriori corrected data we get for all stations (except Arrival Heights) total smoothing errors that are smaller than 1 %.

The relatively low DOFS values for Arrival Heights are explained by the lower signal to noise ratio of Arrival Heights spectra. Arrival Heights is the only site within our study where a Bruker 120M IFS is deployed. All the other sites use Bruker 120HR or 125HR, which offer higher signal to noise ratio as well as better ILS stability than the Arrival Heights 120M. For about 50 % of all Arrival Heights observations we get DOFS values of below 2.0. We exclude the respective spectra from this study, since they make independent lower tropospheric CH_4 retrievals rather difficult. The mean DOFS value for the remaining observations is 2.14, which allows determination of a lower tropospheric column-averaged CH_4 with a smoothing error of typically 1.1 % (but only if the a posteriori correction is applied).

We calculate the statistical and systematic errors for the uncertainty assumptions as listed in Table 2. The statistical errors sum up to about 1 % and are dominated by baseline uncertainties and measurement noise. We estimate a systematic error of about 2.5 %, which almost exclusively reflects the uncertainty in the spectroscopic CH_4 parameters. The a posteriori correction has nearly no effect on the statistical and systematic errors.

The values we report in Table 3 are for one individual measurement, which takes about 5–10 min. At most sites, several measurements are made per day and the statistical errors will be much smaller for the daily averages. The precision for daily mean data is likely better than 0.5 % at all sites (statistical error value of Table 3 multiplied by $1/\sqrt{N}$, with N being the number of measurements).

AMTD
7, 633–701, 2014

3 Pairing the ground-based FTIR and surface in-situ datasets

3.1 Surface in-situ measurement sites

We use surface in-situ CH_4 measurements obtained at different globally distributed sites. The data have been acquired by different institutions (please refer to Table 4). All of these sites are part of the GAW programme, which has been established by the World Meteorological Organization (WMO) in order to ensure consistent high quality standards. All GAW CH_4 site measurements are calibrated to the NOAA04 standard scale (Dlugokencky et al., 2005). Via this program, the activities of the observational in-situ network are coordinated: realisation of station audits, development of standard operational procedures or measurement guidelines, etc. The GAW data are publicly available through the World Data Center for Greenhouses Gases website (WDCGG, http://ds.data.jma.go.jp/gmd/wdcgg/).

The majority of the in-situ stations measure CH_4 by gas chromatography (GC) techniques with flame ionization detection (FID). This technique has been widely used by the in-situ community. In recent years, optical techniques like cavity ring-down spectroscopy (CDRS) or in-situ FTIR analysers have been introduced, showing similar or even better precisions than the traditional GC systems (e.g. Winderlich et al., 2010; Griffith et al., 2012; Hammer et al., 2013). The GAW CH_4 data are generally submitted to the WDCGG as hourly, daily and/or monthly mean and/or as event sampled data. Table 4 summarizes some information and Fig. 2 depicts the location of the in-situ stations that take part in our study.

The GAW CH_4 data are very high quality (compatibility between laboratories of ±2 ppb). However, even if the stations in the GAW network are chosen such that the observed atmospheric composition is regionally representative and usually free of significant local influences they can be affected by local small-scale processes (e.g. small-scale turbulences, very local sources and sinks) and therefore they are not always representative for background conditions. Only under some atmospheric situations we can

AMTD
7, 633–701, 2014

expect that the CH_4 surface in-situ data are representative for tropospheric regional-scale signals and thus comparable to the FTIR data.

To obtain in-situ time series from the GAW data that are representative of regional-scale signals, we apply a series of site specific filters. Figure 7 shows the paired FTIR (red stars) and the filtered regional-scale GAW (black squares) time series for each station. The WACCM apriori values used for the FTIR retrievals are shown as green lines. Please note that there are much more GAW regional-scale data points for the Izaña and Karlsruhe FTIR sites than for the other sites, since for the Izaña and Karlruhe sites we can reconstruct regional-scale GAW data on a daily time scale and for the other sites only on a monthly time scale. Details on the site specific GAW data filtering are explained in the following subsections.

We think that it is important to state here a fundamental difference between the GAW in-situ data and remote sensing data. The in-situ measurements provide pure, precise, and accurate CH_4 data (CH_4 is directly measured and referenced to WMO standards). On the contrary, a remote sensing system like the ground-based FTIR, measures spectral radiances, which are then interpreted with respect to the tropospheric CH_4 signal. This means that the FTIR CH_4 product is a mere proxy for the tropospheric CH_4 state, not to be confused with the true actual tropospheric CH_4 value.

3.2 FTIR Izaña vs. in-situ Izaña

Izaña is a subtropical high mountain observatory located on the Canary Island of Tenerife, Spain at 2367 m a.s.l. The NDACC FTIR has been in operation continuously since 1999 when a Bruker IFS 120M was installed. In March 2005 the instrument was replaced by a Bruker IFS 125HR. A good agreement between instruments has been found during an intercomparison campaign of few months (Sepúlveda et al., 2012; García et al., 2012). In this study we present results for the 2007–2012 period. On average we work with 70.2 days of FTIR measurements per year (251.2 measurements per year).

AMTD
7, 633–701, 2014

The in-situ CH_4 equipment is located only few tens of meters apart from the FTIR. It has measured in-situ CH_4 amounts by the gas chromatography technique with Flame Ionization Detection (GC-FID) continuously since 1984, and since then the data have been uploaded to the WDCGG. See Gomez-Pelaez and Ramos (2011) and references therein for information about the measurement system and the raw data processing scheme used in this global GAW site. Izaña is usually located above a strong subtropical temperature inversion layer. During daytime the strong diurnal insolation generates a slight upslope flow of air originating from below the inversion layer, but during night-time the airmass at Izaña is well representative of the free troposphere (or at least of the lower part of the free troposphere). Due to this special situation we only work with Izaña's GAW CH_4 night-time data (from 20:00 UTC to 08:00 UTC), i.e. we work only with about 50 % of all available hourly mean data. This filter does typically provide one nighttime mean value every 24 h (typically 365 days of in-situ measurements per year). We calculate the GAW CH_4 mean of two consecutive night mean values and pair it with the FTIR daily median of the enclosed day. In addition we calculate a representative daily mean FTIR measurement time (mean time of the used FTIR data ensemble) and require that the FTIR's mean measurement time is between 10:00 UTC and 18:00 UTC (i.e. we exclude days when FTIR data have only been measured very early in the morning or very late in the evening).

3.3 FTIR Karlsruhe vs. in-situ Schauinsland

The Karlsruhe FTIR instrument, a Bruker IFS 125HR, is located in a continental flat terrain inside the Karlsruhe Institute of Technology (KIT), Campus North, Germany at 110 m a.s.l. It has been an official TCCON (Total Carbon Column Observing Network) station since 2010 and also measures down to the mid-infrared ($\approx 2000\,cm^{-1}$), a region that is traditionally covered by NDACC spectrometers. Information about the Karlsruhe instrument can be found in Gisi et al. (2011). On average we work with 104 days of FTIR measurements per year (462.3 measurements per year).

AMTD
7, 633–701, 2014

The closest GAW station that provides continuous in-situ CH_4 data is Schauinsland at 1200 m a.s.l., which is located about 130 km south of Karlsruhe. The station is situated on a mountain ridge in the Black Forest. During night the station is usually above the boundary layer, while during daytime, particularly in summer, the station mostly lies within the convective boundary layer. It has measured in-situ CH_4 amounts by GC-FID continuously since 1991.

In order to get in-situ data representative of regional-scale CH_4 signals, we have to filter the Schauinsland GAW CH_4 measurements (otherwise the data are strongly affected by local small-scale signals). A simple method consists in using local nighttime values (e.g. the nine hours between 22:00 and 07:00) and restrict on observation made at high wind-speed ($> 4\,m\,s^{-1}$). The nighttime filter removes about 60 % of all hourly data. The wind filter removes another 60 %. The two filters together remove almost 85 % of all available hourly data. This is a very high number and leaves us with only 35 % of all measurement days. In addition, we find that this filter does still not reasonably eliminate all the expected local small-scale signals (see Fig. A5 of Appendix A).

For this paper we developed a new method for detecting the regional-scale signals in the surface in-situ CH_4 data. It consists in combining the surface in-situ CH_4 data measured at two Central European sites, Schauinsland and Jungfraujoch. Jungfraujoch is a high mountain observatory located in the Swiss Alps at 3580 m a.s.l., about 150 km south of Schauinsland (see Fig. 2). We define the Schauinsland CH_4 background signal as the signal that remains after requiring common variability in the Schauinsland and Jungfraujoch data. This filter removes about 50 % of all available hourly mean data (leaves us with data for 65 % of all measurement days). The amount of removed data is significantly smaller than when using the nighttime/wind filter. Furthermore, the local small-scale signals are very effectively eliminated, thereby allowing the reconstruction of regional-scale in-situ signals. Please refer to Appendix A for details about this filter method.

We calculate daily medians and a representative daily mean measurement time (mean time of the used data ensemble) from the filtered in-situ data. The GAW daily

AMTD
7, 633–701, 2014

medians are then paired with the FTIR daily medians, but only if the GAW and FTIR representative measurement times agree within 6 h (i.e. we do not compare the data if, for instance, one instrument measures only in the morning and the other one only in the evening).

3.4 FTIR Eureka vs. in-situ Alert

The NDACC FTIR Eureka and GAW Alert stations are located on Ellesmere Island/Nunavut in the Canadian Arctic. The NDACC FTIR instrument is located at the Polar Environment Atmospheric Research Laboratory (PEARL) at 610 m a.s.l., operating throughout the sunlit period of the year (mid-February to mid-October). Its activities started in 1993 with a Bomem DA8 FTIR, which was replaced in July 2006 by a Bruker 125HR FTIR. In this study we present results only for the latter instrument and for a period of 6 yr. On average we work with 58 days of FTIR measurements per year (257 measurements per year). Details of the NDACC FTIR instrument, observations, and the PEARL site can be found in Batchelor et al. (2009).

The GAW measurements are made at the Dr. Neil Trivett GAW Observatory at Alert situated at 210 m a.s.l. on the northeastern tip of the island (about 460 km north of PEARL). It is the most northerly site within the GAW network and has measured in-situ CH_4 amounts by GC-FID continuously since 1988.

Both sites are far away from major anthropogenic activities and therefore we assume that they are well-suited for measuring regional-scale CH_4 signals. We work with the hourly GAW data but remove data where the standard deviation is greater than 0.5 % (hourly data are typically calculated from 4–5 individual measurements). This filter only removes 1 % of all available hourly mean data. Then, we calculate daily medians from the remaining hourly data, retaining data if the number of hourly data points is larger or equal than six and the respective standard deviation is smaller or equal than 1 %. From the remaining daily medians we calculate monthly medians and pair them with the coincident FTIR monthly medians. Here we compare only monthly and not daily datasets since there is a significant distance between the FTIR and the GAW sites

AMTD
7, 633–701, 2014

and we cannot reconstruct GAW regional-scale signals on a daily time scale that are representative for the FTIR site.

3.5 FTIR Ny-Ålesund vs. in-situ Ny-Ålesund

Ny-Ålesund is a small Norwegian settlement located in the north-west part of the island of Spitsbergen in the Svalbard archipelago, European Arctic. The NDACC FTIR experiment is situated at 21 m a.s.l. The FTIR spectra have been measured from the end of March to the end of September every year since 1990. In 1995, the Bruker 120M was replaced by a 120HR. We present results for the period 2005 to 2010. On average we work with 23 days of FTIR measurements per year (45 measurements per year). Details of the NDACC FTIR instrument and site can be found in Notholt et al. (1995).

The Ny-Ålesund GAW in-situ station is located slightly south from the FTIR on a small plateau of the Zeppelin Mountain at 475 m a.s.l. The GAW data are generally not influenced by local pollution from the settlement. Several flasks are collected per month (there are no CH_4 measurements on a daily basis) and all the samples are analysed for CH_4 at NOAA ESRL since 1994. We do not filter these in-situ data. We pair the GAW monthly mean data with the coincident FTIR monthly medians.

3.6 FTIR Kiruna vs. in-situ Pallas-Sammaltunturi

The NDACC FTIR Kiruna instrument is located at the Swedish Institute of Space Physics in the North of Sweden at 419 m a.s.l. A Bruker IFS 120HR has been operated continuously since 1996 and in July 2007 the instrument was upgraded to a 125HR. Information about the instrument can be found in Blumenstock et al. (2006). The period covered in this study is from 2004 to 2010. On average we work with 51 days of FTIR measurements per year (98.9 measurements per year).

The closest GAW in-situ site that provides CH_4 data is Pallas-Sammaltunturi situated in northern Finland at 560 m a.s.l. and about 250 km east of the Kiruna NDACC FTIR. Pallas-Sammaltunturi is on the top of a hill about 100 m above the tree line and it

AMTD
7, 633–701, 2014

is considered free of large local and regional pollution sources. From 2004 to 2008, the in-situ CH_4 amounts were measured by the traditional GC-FID system but since January 2009 the CDRS optical technique has been applied.

The in-situ station provides hourly data and in order to obtain the large-scale monthly median signal, we perform the same data treatment as for the Alert site (please refer to Sect. 3.4), i.e. there are only about 1 % of all available hourly data removed. We pair the GAW monthly medians with the coincident FTIR monthly medians. Here we compare only monthly and not daily datasets since there is a significant distance between the FTIR and the GAW sites.

3.7 FTIR Bremen vs. in-situ Mace Head

The NDACC FTIR Bremen instrument is located in the Institute of Environmental Physics at the University of Bremen, Germany at an altitude of 27 m a.s.l. A Bruker 125HR has been operated since June 2004. We work with data until 2011. On average we work with 29 days of FTIR measurements per year (50.9 measurements per year). Information about the instrument can be found in Velazco et al. (2007).

The Mace Head Research Station is located on the west coast of Ireland, County Galway at 5 m a.s.l., and about 1000 km east from Bremen. It is representative of background marine boundary layer conditions when the air masses arrive from the North Atlantic ocean (on average over 60 %, from meteorological records). The in-situ CH_4 amounts has been measured by GC-FID system. The station provides event and monthly mean data since 1987. We do not apply any filter to the dataset. We pair the GAW monthly mean data with the coincident FTIR monthly medians since there is a significant distance between the FTIR and the GAW sites.

3.8 FTIR Wollongong vs. in-situ Cape Grim

The NDACC FTIR Wollongong site is located at the University of Wollongong, Australia at 30 m a.s.l. Its activities started in 1994 with a Bomem DA3, which was upgraded to

AMTD
7, 633–701, 2014

a Bomen DA8 in 1996. Since 2007, a Bruker IFS 125HR has been in operation. Here, we only use data from this new instrument and for a period of 5 yr. On average we work with 66 days of FTIR measurements per year (350 measurements per year). Details of the current FTIR instrument can be found in Kohlhepp et al. (2012).

For our comparison with the FTIR data, we use the GAW CH_4 measurements acquired at the Cape Grim Baseline Air Pollution Station. This site is located in the northwestern point of Tasmania, Australia, at 94 m a.s.l. and about 1000 km south of Wollongong. The air that arrives at Cape Grim station from the southwest is essentially marine air. The in-situ GAW CH_4 measurements started in 1981 with a GC-FID system. For this work we use the values measured continuously since January 2007.

In order to ensure that the Cape Grim CH_4 signals are also representative for the Wollongong area we look in addition at data measured at Cape Ferguson, located towards the northest tip of Australia at 2 m a.s.l. and about 1500 km north of Wollongong. There flasks are collected several times per month since 1991. We combine the data gathered at two different GAW stations and look for common variability. This method is similar to the one we use for Central Europe (see Appendix A). In the case of Australia we first calculate daily means from the continuous Cape Grim data and for the several times per month acquired Cape Ferguson data. Then we pair the daily coincidences from both stations. Between August 2007 and August 2011 there are 76 daily coincidences. This number is determined by the rather low number of Cape Ferguson data. We define the in-situ CH_4 regional-scale signal as the signal that remains after requiring common variability in these coincident Cape Grim and Cape Ferguson data. This filter leaves as with 66 Cape Grim daily mean data (i.e. about 15 % of the data are filtered out) that should be well representative for the whole east coast of Australia (extension from north to south of 2500 km).

Finally we calculate the monthly medians from the retained Cape Grim data and pair them with the coincident FTIR monthly medians. Here we compare only monthly and not daily datasets since there is a significant distance between the FTIR and the GAW sites.

AMTD
7, 633–701, 2014

3.9 FTIR Lauder vs. in-situ Lauder

The NDACC FTIR Lauder experiment is located at the National Institute of Water and Atmospheric Research (NIWA) station in Central Otago, New Zealand at an altitude of 370 m a.s.l. The ground-based remote sensing FTIR activities started in 1986 with a Bomem DA2 operated in campaign mode. Long term full time measurements started in 1990 with the temporary instalment of a Bruker 120HR which was replaced in late 1991 with a Bruker 120M (Griffith et al., 2003). Since 2001 a later model Bruker 120HR has been in operation. We present results for the period 2007 to 2012. On average we work with 52 days of measurements per year (87 measurements per year). Details of the current FTIR instrument can be found in Morgenstern et al. (2012).

Surface in-situ CH_4 measurements at Lauder started in 2007 with the installation of an in-situ FTIR spectrometer trace gas analyser. Since here we present the Lauder in-situ FTIR data for the first time in a peer review article we provide some details on its measurement principle and data quality in the Appendix B.

For the purposes of this study in order to obtain a regional-scale CH_4 signal we filter the in-situ data for conditions that are indicative for a well-mixed boundary layer: first, we only work with afternoon data (hourly mean between 15:00 LT and 16:00 LT, if standard deviation is within 0.5 %). This removes more than 96 % of all available data. Second, we require the wind speed to be above 5 m s^{-1}, which removes another 72 %. We apply a filter that removes in total almost 99 % of all available in-situ data. For the remaining data we only have 19 daily coincidences of the in-situ measurements with the ground-based FTIR mesurements. This is a very low number and we decided to work with monthly coincidences. For this purpose we calculate monthly medians from the remaining in-situ data and pair it with the coinciding FTIR monthly medians. Please note that we have 47 monthly coincidences but only 19 daily coincidences since we define as a monthly coincidence each month that has at least one in-situ and one FTIR measurement at any day during the month, whereas for a daily coincidence we require that the in-situ and the ground-based FTIR data are obtained at exactly the same day.

AMTD
7, 633–701, 2014

3.10 FTIR Arrival Height vs. in-situ Arrival Height

The Arrival Heights atmospheric laboratory is located 3 km north of McMurdo and Scott Base stations on Hut Point Peninsula, Ross Island, Antarctica at 184 m a.s.l. Campaign based MIR-FTIR measurements started in 1988 when NIWA operated a Bomen DA2 FTIR in the austral spring. Full time measurements were initiated in 1991 with an Eocom 7101 FTIR and in 1996 a Bruker 120M replaced the Eocom. Unlike the prior FTIR systems the Bruker 120M contains a complete NDACC compliant filter set allowing the collection of solar spectra (August to March) over the wavenumber range 700 cm^{-1} to 4200 cm^{-1}. Details of the Arrival Heights NDACC site and FTIR instrumentation can be found in Wood et al. (2002). For this study we work with the spectra that have been measured since 2002 until 2011. On average we work with 10.5 days of measurements per year (11.5 measurements per year).

The GAW CH_4 data is measured by flasks since 1989 (Lowe et al., 1997). The fortnightly flask samples are taken only when the wind is from the northerly direction and the wind speed is greater than 5 $m\,s^{-1}$ (there are no CH_4 measurements on a daily basis). This is to avoid any possible contamination from Scott Base and McMurdo station anthropogenic emissions. We use these data only if the event data are calculated as the mean of at least five individual measurements and if the respective standard deviation is within 0.5 %. The removes about 5 % of all the data available on the GAW database. From these remaining dataset we calculate monthly medians and pair it with the FTIR monthly medians.

4 Comparison of the ground-based FTIR and surface in-situ datasets

Table 5 summarizes the sites involved in the comparison, the time scale of the compared data, the filters applied for ensuring regional-scale GAW data, and the number of coincidences.

AMTD
7, 633–701, 2014

4.1 Daily datasets

For Izaña and Karlsruhe we have daily GAW in-situ data that are representative of regional-scale CH_4 signals (see explanation in Sects. 3.2 and 3.3). This offers unique opportunities for extensive comparison studies between the GAW in-situ and the Izaña and Karlsruhe FTIR remote sensing data. Figure 7 gives an overview of this large amount of data, covering almost six years for Izaña (2007–2012) and three years for Karlsruhe (2010–2012).

Figure 8 shows correlation plots for the daily coincidences. For Izaña there are 225 and for Karlsruhe there are 162 daily coincidences. We observe a reasonable correlation. However, the FTIR values are systematically higher than the GAW in-situ values. This systematic difference of about 2 % is very likely due to uncertainties in the applied spectroscopic parameters of CH_4. As mentioned in Sect. 2.2, further improvement of the CH_4 spectroscopic parameters is the subject of a current project.

For analysing the time series on different time scales we fit the measured time series to a time series model, which is similar to the one used in Gardiner et al. (2008); Sepúlveda et al. (2012). The model considers a mean CH_4 value and CH_4 variations on different time scales: a linear trend, intra-annual variations (Fourier series with three frequencies and phases), and inter-annual variations (Fourier series with frequencies lower than $1\,yr^{-1}$). For this analysis we work with the CH_4 values in the logarithmic scale. Since the tropospheric CH_4 variations (typically smaller than 50 ppb) are much smaller than the climatological CH_4 reference value (typically about 1850 ppb) we can interpret the variations on logarithmic scale ($\Delta \ln[CH_4]$) as the variations relative to the climatological reference value ($\Delta[CH_4]/[CH_4]$):

$$\Delta \ln[CH_4] \approx \Delta[CH_4]/[CH_4] \quad (17)$$

In order to investigate de-trended seasonal cycles we reconstruct a time series that only considers variation on the time scales longer than the seasonal cycle, i.e. we use the fit results obtained for the mean CH_4 value, the linear trend, and the inter-annual variations. This reconstructed time series does not reflect seasonal variations

AMTD
7, 633–701, 2014

and can be interpreted as the climatological long-term reference. We subtract it from the measured time series. Since we work with $\ln[CH_4]$ values the difference can be interpreted as the seasonal variation relative to the climatological long-term reference (see approximation 17). Then we calculate the mean and standard errors of the mean for these differences for each month (independently from the year). These mean values and standard errors of the mean are shown as the dots and error bars in Fig. 9. They represent the de-trended seasonal cycles (GAW: black squares; FTIR: red stars) relative to the climatological long-term reference. For both sites, we find generally good agreement between the seasonal cycles of FTIR and GAW (amplitude and phase). The shapes of the seasonal cycles at Izaña and Karlsruhe are different. At Izaña we observe no significant CH_4 changes between November and May and a rather sharp minimum in July. At Karlsruhe the tropospheric CH_4 mole fraction decrease continuously between February and August, when the minimum value is reached. These differences between the seasonal cycles at the two sites are observed consistently in the FTIR and the GAW data.

In addition to the seasonal time scale we look on day-to-day and long-term (biannual) time scales. For the separation into the different time scales we use the aforementioned time series model. The day-to-day time scale signal is calculated as the difference (on logarithmic scale) between the measured time series and the modeled time series (whereby all fitted time scales are considered: mean value, linear trend, seasonal cycle, and inter-annual cycle). Thereby we include all the variations (linear trend, seasonal cycle, and inter-annual cycle) when defining the climatological CH_4 reference. The so-calculated day-to-day time scale variations represent the variations that take place within a few weeks, relative to the this climatological CH_4 reference (see approximation 17).

In order to calculate the long-term (biannual) time scale signal we reconstructed a time series that only considers the fit results obtained for the mean CH_4 and the seasonal cycle and define it as climatological reference. Then we subtract it from the measured time series and obtain CH_4 values relative to the climatological reference

AMTD
7, 633–701, 2014

(see approximation 17). By this measure we get a de-seasonalised time series, for which we then calculate the biannual mean values.

In Fig. 10 we correlate the different time scale signals obtained for the GAW and the FTIR data. We find a good consistency for the correlations for all the different time scales. This clearly documents that GAW and NDACC FTIR consistently detect intra-monthly, seasonal, and long-term CH_4 variations.

4.2 Monthly datasets

For the NDACC FTIR sites of Eureka, Ny-Ålesund, Kiruna, Bremen, Wollongong, and Arrival Heights we cannot calculate daily GAW in-situ data that are representative for regional-scale CH_4 signals. Due to the different sampling characteristics of FTIR and GAW we cannot perform meaningful inter-comparisons on a daily basis for these sites and therefore we restrict the inter-comparison to monthly means, i.e. to large-scale signals. We then compare the GAW CH_4 monthly medians to the monthly FTIR medians, but only if the mean measurement times (mean time of the used daily data ensembles) do not differ by more than 15 days. An overview of the data amount that is compared is given in Fig. 7.

Figures 11–13 show the respective FTIR vs. GAW comparisons analogous to Figs. 8–10. The number of monthly coincidences are naturally smaller than the number of daily coincidences. For instance we have only 65 monthly coincidences for Bremen and 21 monthly coincidences for Arrival Heights. We observe essentially the same as for the Izaña and Karlsruhe comparisons: good correlations (on different time scales), reasonable agreement of seasonal cycles, and a systematic difference of about 2 %.

In particular for Arrival Heights we observe that the FTIR seasonal cycle has a significantly larger amplitude than in-situ seasonal cycle (see Figs. 7 and 12). This is mainly due to the interference from the UTLS. At Arrival Heights the vertical resolution is more limited than at other sites (i.e. resulting in a lower DOFS) and in addition the UTLS is rather close to the FTIR, i.e. we cannot completely eliminate influences of the UTLS on our tropospheric FTIR product. There is an anti-correlation between the real UTLS

AMTD
7, 633–701, 2014

CH_4 and the retrieved tropospheric FTIR CH_4. This is predicted by the kernels (see right panel in Fig. 4) and the reason for the large amplitude as observed by the FTIR. In summer (high CH_4 in the UTLS), the retrieved tropospheric FTIR CH_4 is too low and in winter (low CH_4 in the UTLS) it is too high. The a posteriori correction method reduces this effect but cannot completely eliminate it (because of the low DOFS). Something similar is observed for Ny-Ålesund.

4.3 Network-wide data consistency

Latitudinal gradients of CH_4 contain valuable source/sink information. In this subsection we examine whether the FTIR and GAW data observe similar site specific long-term CH_4 evolutions. For this purpose we look at de-seasonalised biannual mean data. Because the WACCM apriori data are station specific, i.e. they change from FTIR station to FTIR station, the differences between the FTIR data obtained at the different stations are due to a combination of the differences in the applied apriori data and the differences actually measured by the FTIR instruments. In order to reduce the influence of the apriori on our consistency assessment, we remove the WACCM apriori data and compare FTIR-WACCM with GAW-WACCM for each station. Hence we investigate whether the FTIR and GAW measurements allow a consistent improvement of a global model such as WACCM.

Since the seasonal cycles have been well studied in the previous sections and in order to investigate the average situation we work here with de-seasonalised biannual mean GAW and FTIR data, i.e. we remove the seasonal cycles as plotted in Figs. 9 and 12. Then we calculate the differences to the station specific WACCM data (i.e. calculate GAW-WACCM and FTIR-WACCM). This is done on a logarithmic scale. Since the CH_4 values are much larger than the difference with respect to the WACCM model approximation 17 applies and we can interpret the difference on logarithmic scale as the relative difference. In Fig. 14 we correlate the GAW-WACCM and FTIR-WACCM data. Both the GAW and FTIR data show similar differences with respect to the WACCM climatological mean data. The statistic for the

AMTD
7, 633–701, 2014

difference ([GAW – WACCM] – [FTIR – WACCM] = [GAW] – [FTIR]) for the deseasonalised biannual means for the different sites is 2.18 % ± 0.65 % (mean ± standard deviation). We observe that the data are described well by a straight line, meaning that both networks (GAW in-situ and NDACC FTIR) observe similar differences with respect to the model. Figure 14 also show a linear regression line (yellow), for which we obtain a correlation coefficient R^2 of 0.69. We think that this is a conservative documentation of the data consistency since it still has to be taken into account that some of the GAW data are measured several hundreds of kilometres away from the FTIR sites, and that local small-scale effects on the GAW data cannot be fully excluded.

As already observed and discussed in previous sections there is a systematic difference of about 2 % (the dashed line is the diagonal + 2 %). This systematic difference can be removed by calibrating the CH_4 spectroscopy to the GAW observations (calibration factor of 0.98). The calibration factor of 0.98 is also found in Wunch et al. (2010) showing an analogous comparison between TCCON CH_4 and total column in-situ measurements on the NOAA scale. Although, in this study and in the work of Wunch et al. (2010) different quantities are compared (TCCON vs. NDACC and total column vs. surface in-situ), we think that this does add some good weight to the spectroscopy vs. in-situ CH_4 comparison in general (e.g. if the line strengths were off by the same 2 % in both regions).

5 Conclusions

In this work we present a lower tropospheric regional-scale CH_4 product obtained from the ground-based FTIR remote sensing measurements made within the NDACC. The work extends the study of Sepúlveda et al. (2012), which was limited to the subtropical site of Izaña, to a set of nine globally distributed FTIR sites situated in polar regions, the mid-latitudes, and the subtropics. In order to minimise potential humidity interferences at humid sites like Wollongong, Bremen, or Karlsruhe, we slightly modify our spectral microwindow selection. Furthermore we use new spectroscopic CH_4 parameters,

AMTD
7, 633–701, 2014

which are currently produced within a project of the Deutsche Forschungsgemeinschaft (D. Dubravica and F. Hase, personal communications, 2012, work still in progress).

We demonstrate that the retrieved lower tropospheric CH_4 mole fraction can be significantly affected by CH_4 variations in the UTLS caused by tropopause altitude shifts. This is a severe problem and strongly compromises the scientific value of the tropospheric CH_4 data product. For instance, it means that the retrieved lower tropospheric seasonal cycle might mainly reflect the seasonal cycle of the tropopause altitude thus offering rather limited information for investigating CH_4 source/sink processes. We show that this dependency on UTLS variations can be significantly reduced by an a posteriori correction method. The correction consists of a simple matrix multiplication applied to the retrieved CH_4 state and is strongly recommended for polar sites. When applying this correction, we demonstrate that the NDACC FTIR experiments can observe lower tropospheric CH_4 mole fraction largely independent of the variation in the UTLS region. We estimate a precision for the daily mean data of about 0.5 %. We estimate a systematic error of about 2.5 % (Table 3) due to the uncertainty in the applied spectroscopic parameters (intensity and pressure broadening coefficient) of CH_4.

In contrast to the pure CH_4 measurements provided by GAW, the remote sensing CH_4 product is a mere proxy for the true actual tropospheric CH_4 value. This paper uses the GAW data in order to demonstrate that the NDACC FTIR CH_4 proxy reasonably picks up the actual CH_4 variability and so it can be recommended, for instance, for the purpose of satellite validation or for assimilation into a model. In these applications the limitations introduced by the applied constraints can be taken properly into account.

The Izaña nighttime GAW data are well representative for the lower free troposphere (subtropical island on a mountain). At Karlsruhe we use Schauinsland data, whose regional-scale signal is obtained by requiring correlation to the Jungfraujoch data. For this reason we think that for the Izaña and Karlsruhe NDACC FTIR site, we can generate a regional-scale GAW signal on a daily time scale that serves as a reasonable reference for the FTIR data. We show that both the remote sensing and in-situ data observe very similar lower tropospheric regional-scale CH_4 signals. The good agreement

AMTD
7, 633–701, 2014

is demonstrated for the different time scales that are interesting for CH_4 source/sink research: daily, seasonal, and long-term biannual mean evolution. For the other seven sites, we compare FTIR and regional-scale GAW data on a monthly time scale. The comparisons for these sites confirm the results obtained for the Izaña and Karlsruhe study. We demonstrate that both networks observe consistent latitudinal CH_4 gradients. The observed systematic difference of about 2 % is within the estimated systematic error due to the uncertainty of the spectroscopic parameters. This systematic difference can be removed by calibrating the CH_4 spectroscopy to the GAW observations (calibration factor of 0.98).

Appendix A

Combination of data from two nearby GAW stations

Central Europe offers the opportunity to combine two GAW datasets measured at two nearby stations at different altitudes within the free troposphere. The two stations are Schauinsland (47.97° N, 24.12° E, 1210 m a.s.l.) and Jungfraujoch (46.55° N, 7.99° E, 3580 m a.s.l.). Their location is depicted together with the location of the Karlsruhe FTIR instrument in Fig. A1. The stations should measure the same large-scale CH_4 signal when no local influences affect them. We combine the two central European GAW datasets to filter out the small-scale signals and thus, obtain a regional-scale signal.

The applied method is as follows:

- we pair the original hourly mean data of both stations (this large dataset is shown in Fig. A2).
- We calculate the time series of the differences between the Schauinsland and Jungfraujoch data.

AMTD
7, 633–701, 2014

– We fit a modeled time series to the measured difference. The model considers a systematic difference and an annual cycle of the difference.

– We calculate the residual (difference between modeled and observed differences).

– We only retain Schauinsland data when this residual is smaller than 1 %.

This data treatment gives some very interesting insight into Central European's CH_4 variations. Figure A3 shows that the annual CH_4 cycles at both stations are not in phase and that the Schauinsland mole fraction are systematically about 2 % larger than the Jungfraujoch mole fraction. Both can be expected due to the relatively high altitude of Jungfraujoch compared to Schauinsland.

Figure A4 shows an example for the behaviour of this filter for November 2010. After removing the local signals we can still observe some increased CH_4 mole fraction with a periodicity of about 10 days. We think that these are regional-scale CH_4 signals that are related to the synoptical-scale situation of Europe in this period.

Figure A5 shows the advantage of this filter in comparison to another possible filter method. It shows comparisons of Schauinsland in-situ data to coincident Karlsruhe FTIR data. The left panel for unfiltered in-situ data, the middle panel uses nighttime data filtered additionally by the wind criteria (wind speed $> 4\,m\,s^{-1}$), and the right panel shows the situation when applying the filter discussed here, which searches for common signals at Schauinsland and Jungfraujoch. We apply the filters on the hourly mean data, where the nighttime/wind filter removes about 85 % of all data and then calculate daily medians whenever there remains at least one hourly mean data for the day after filtering. The nighttime/wind filtered dataset leads to only 90 daily coincidences, i.e. about 65 % less daily coincidences than the unfiltered dataset, where we have 258 daily coincidences. The filter that works with common signals at Schauinsland and Jungfraujoch removes about 50 % of all hourly mean data and it leads to about 38 % less daily mean data (N = 162) than the unfiltered dataset (N = 258), i.e. it removes significantly less data than the nighttime/wind filter. When applying the filter for common signals

AMTD
7, 633–701, 2014

we observe a reasonable correlation between the Schauinsland in-situ and the Karlsruhe FTIR data (correlation coefficient of about 0.6). For the nighttime/wind filter the respective correlation coefficient is 0.26 (if we remove an outlier it is 0.47).

In summary, the here proposed filter for common signals removes significantly less data than the simple nighttime/wind filter. In addition it seems to very efficiently remove local small-scale signals, whereas the simple nighttime/filter does not that efficiently remove these local small-scale signals.

Appendix B

The Lauder in-situ FTIR dataset

The Lauder FTIR analyser is a prototype of that described in Griffith et al. (2012); Hammer et al. (2013). Continuous 10 min measurements of CO_2, CH_4, CO and N_2O are made from air drawn from an inlet located at the top of a 10 m mast. A roughing pump delivers sample air to a manifold at a rate of 10 L min^{-1} from this the FTIR analyser draws off sample air at 0.5 L min^{-1}. Daily measurements of a single working tank (prepared by NIWA-Gaslab, New Zealand) allow calibration of the atmospheric sample to the NOAA04 CH_4 scale. The precision of the measurements is 0.2 ppb. Due to the large operational pressure range a residual pressure sensitivity (Hammer et al., 2013) of 0.0285 ppb hPa^{-1} was experimentally derived and applied to sample measurements.

To assess the performance of the FTIR analyser against a standard in-situ measurement technique fortnightly flask samples have been taken at Lauder since mid-2009. Analysed at the NIWA-Gaslab, the resultant GC/FID derived CH_4 flask sample concentrations are also calibrated to the NOAA04 scale. A comparison of 71 flask samples and coincident FTIR analyser measurements over the period 2009 to 2013 show a −0.67 ppb bias (with a 1 sigma sd of 2.03 ppb) in the FTIR analyser measurements. This bias is not seasonally dependent and within the GAW network comparability recommended limit of ±2 ppb (WMO, 2012).

AMTD
7, 633–701, 2014

Additionally, in accordance with the recommendations of a WMO audit of the Lauder site GAW measurements conducted in 2010 (Zellweger et al., 2010) it is envisaged both the Lauder FTIR analyser and flask CH_4 in-situ datasets will be submitted to the GAW WDCGG database in the first half of 2014.

Acknowledgements. We would like to thank the many different technicians, PhD students, post-docs, and scientists from the different research groups that have been involved in the NDACC-FTIR activities during the last two decades. Thanks to their excellent work (maintenance, calibration, observation activities, etc.) high quality long-term datasets can be generated.

The Eureka measurements were made at the Polar Environment Atmospheric Research Laboratory (PEARL) by the Canadian Network for the Detection of Atmospheric Change (CANDAC), led by James R. Drummond, and in part by the Canadian Arctic ACE Validation Campaigns, led by Kaley A. Walker. They were supported by the AIF/NSRIT, CFI, CFCAS, CSA, EC, GOC-IPY, NSERC, NSTP, OIT, PCSP, and ORF.

The authors wish to thank Rebecca Batchelor, Rodica Lindenmaier, PEARL site manager Pierre F. Fogal, the CANDAC operators, and the staff at Environment Canadas Eureka weather station for their contributions to data acquisition, and logistical and on-site support.

We thank the Alfred Wegener Institut Bremerhaven for support in using the AWIPEV research base, Spitsbergen, Norway.

We would like acknowledge funding from the EU-Project InGOS and the Senate of Bremen for supporting the measurement program at Bremen.

We would like to thank Uwe Raffalski and Peter Völger for technical support at IRF Kiruna.

Measurements at Wollongong are supported by the Australian Research Council, grant DP110103118.

We would like to thank Antarctica New Zealand and the Scott Base staff for providing logistical support for the NDACC-FTIR measurement and in-situ program at Arrival Heights. The NIWA measurements at Lauder and Arrival heights is core funded through the Ministry of Business, Innovation and employment. The authors would like to thank Dr Vanessa Sherlock for her input and helpful comments.

The Advanced Global Atmospheric Gases Experiment (AGAGE) is funded by NASA grant NNX11AF17G to MIT. Funding for AGAGE measurements at Mace Head, Ireland comes from the above NASA grant to MIT and the UK Department of Energy and Climate Change. AGAGE measurements at Cape Grim, Tasmania are supported by the above NASA grant to MIT and

AMTD
7, 633–701, 2014

by the Australian Bureau of Meteorology and CSIRO Marine and Atmospheric Research. Flask measurements from Cape Ferguson, Australia are funded by CSIRO Marine and Atmospheric Research.

In-situ CH_4 measurements at Jungfraujoch are run by Empa in collaboration with the Swiss Federal Office for the Environment (FOEN). Empa and FOEN acknowledge the International Foundation High Altitude Research Station Jungfraujoch and Gornegrat (HFSJG) for providing access to Jungfraujoch facilities.

The Izaña in-situ GAW measurements have been carried out and financed by the Izaña Atmospheric Research Center (AEMET).

At Ny-Alesund and Izaña, the FTIR work has received funding from the European Community's Seventh Framework Programme ([FP7/2007–2013]) under grant agreement no. 284421 (see Article II.30. of the Grant Agreement). At Izaña has also received funding from the Ministerio de Economía and Competitividad from Spain for the project CGL2012-37505 (NOVIA project).

This study has strongly benefited from work made in the framework of the project MUSICA, which is funded by the European Research Council under the European Community's Seventh Framework Programme (FP7/2007–2013)/ERC Grant agreement number 256961.

E. Sepúlveda enjoyed a pre-doctoral fellowship thanks to the Spanish Ministry of Education.

AMTD
7, 633–701, 2014

References

Batchelor, R. L., Strong, K., Lindenmaier, R., Mittermeier, R. L., Fast, H., Drummond, J. R., and Fogal, P. F.: A new Bruker IFS 125HR FTIR spectrometer for the Polar Environment Atmospheric Research Laboratory at Eureka, Canada – measurements and comparison with the existing Bomem DA8 spectrometer, J. Atmos. Ocean. Tech., 26, 1328–1340, 2009. 655

Blumenstock, T., Kopp, G., Hase, F., Hochschild, G., Mikuteit, S., Raffalski, U., and Ruhnke, R.: Observation of unusual chlorine activation by ground-based infrared and microwave spectroscopy in the late Arctic winter 2000/01, Atmos. Chem. Phys., 6, 897–905, doi:10.5194/acp-6-897-2006, 2006. 656

Dlugokencky, E. J., Myers, R. C., Lang, P. M., Masarie, K. A., Crotwell, A. M., Thoning, K. W., Hall, B. D., Elkins, J. W., and Steele, L. P.: Conversion of NOAA atmospheric dry air CH_4 mole fractions to a gravimetrically prepared standard scale, J. Geophys. Res., 110, D18, doi:10.1029/2005JD006035, 2005. 651

Dubravica, D., Birk, M., Hase, F., Loos, J., Palm, M., Sadeghi, A., and Wagner, G.: Improved spectroscopic parameters of methane in the MIR for atmospheric remote sensing, in: High Resolution Molecular Spectroscopy 2013 meeting, 25–30 August 2013, Budapest, Hungary, available at: http://lmsd.chem.elte.hu/hrms/abstracts/D16.pdf (last access: 5 December 2013), 2013. 641

García, O. E., Schneider, M., Redondas, A., González, Y., Hase, F., Blumenstock, T., and Sepúlveda, E.: Investigating the long-term evolution of subtropical ozone profiles applying ground-based FTIR spectrometry, Atmos. Meas. Tech., 5, 2917–2931, doi:10.5194/amt-5-2917-2012, 2012. 652

Gardiner, T., Forbes, A., de Mazière, M., Vigouroux, C., Mahieu, E., Demoulin, P., Velazco, V., Notholt, J., Blumenstock, T., Hase, F., Kramer, I., Sussmann, R., Stremme, W., Mellqvist, J., Strandberg, A., Ellingsen, K., and Gauss, M.: Trend analysis of greenhouse gases over Europe measured by a network of ground-based remote FTIR instruments, Atmos. Chem. Phys., 8, 6719–6727, doi:10.5194/acp-8-6719-2008, 2008. 661

Gisi, M., Hase, F., Dohe, S., and Blumenstock, T.: Camtracker: a new camera controlled high precision solar tracker system for FTIR-spectrometers, Atmos. Meas. Tech., 4, 47–54, doi:10.5194/amt-4-47-2011, 2011. 638, 653

AMTD
7, 633–701, 2014

Gomez-Pelaez, A. J. and Ramos, R.: Improvements in the Carbon Dioxide and Methane Continuous Measurement Programs at Izaña Global GAW Station (Spain) during 2007–2009, Report of the 15th WMO/IAEA Meeting of Experts on Carbon Dioxide, Other Greenhouse Gases, and Related Tracer Measurement Techniques, 7–10 September 2009, Jena, Germany, GAW Report number 194, WMO TD 1553, available at: http://www.wmo.int/pages/prog/arep/gaw/gaw-reports.html (last access: 2 February 2012), 2011. 653

Griffith, D. W. T., Jones, N. B., McNamara, B., Walsh, C. P., Bell, W., and Bernardo, C.: Intercomparison of NDSC ground-based solar FTIR measurements of atmospheric gases at Lauder, New Zealand, J. Atmos. Ocean. Tech., 20, 1138–1153, 2003. 659

Griffith, D. W. T., Deutscher, N. M., Caldow, C., Kettlewell, G., Riggenbach, M., and Hammer, S.: A Fourier transform infrared trace gas and isotope analyser for atmospheric applications, Atmos. Meas. Tech., 5, 2481–2498, doi:10.5194/amt-5-2481-2012, 2012. 651, 669

Hammer, S., Griffith, D. W. T., Konrad, G., Vardag, S., Caldow, C., and Levin, I.: Assessment of a multi-species in situ FTIR for precise atmospheric greenhouse gas observations, Atmos. Meas. Tech., 6, 1153–1170, doi:10.5194/amt-6-1153-2013, 2013. 651, 669

Hase, F. and Höpfner, M.: Atmospheric raypath modelling for radiative transfer algorithms, Appl. Optics, 38, 3129–3133, 1999. 639

Hase, F., Blumenstock, T., and Paton-Walsh, C.: Analysis of the instrumental line shape of high-resolution Fourier transform IR spectrometers with gas cell measurements and new retrieval software, Appl. Optics, 38, 3417–3422, 1999. 645

Hase, F., Hanningan, J. W., Coffey, M. T., Goldman, A., Höpfner, M., Jones, N. B., Rinsland, C. P., and Wood, S. W.: Intercomparison of retrieval codes used for the analysis of high-resolution ground-based FTIR measurements, J. Quant. Spectrosc. Ra., 87, 25–52, 2004. 639, 641

Hoinka, P. K.: Statistic of the global tropopause pressure, Mon. Weather Rev., 126, 3303–3325, 1998. 636

Kohlhepp, R., Ruhnke, R., Chipperfield, M. P., De Mazière, M., Notholt, J., Barthlott, S., Batchelor, R. L., Blatherwick, R. D., Blumenstock, Th., Coffey, M. T., Demoulin, P., Fast, H., Feng, W., Goldman, A., Griffith, D. W. T., Hamann, K., Hannigan, J. W., Hase, F., Jones, N. B., Kagawa, A., Kaiser, I., Kasai, Y., Kirner, O., Kouker, W., Lindenmaier, R., Mahieu, E., Mittermeier, R. L., Monge-Sanz, B., Morino, I., Murata, I., Nakajima, H., Palm, M., Paton-Walsh, C., Raffalski, U., Reddmann, Th., Rettinger, M., Rinsland, C. P., Rozanov, E., Schneider, M., Senten, C., Servais, C., Sinnhuber, B.-M., Smale, D., Strong, K., Sussmann, R., Taylor, J. R.,

AMTD
7, 633–701, 2014

Vanhaelewyn, G., Warneke, T., Whaley, C., Wiehle, M., and Wood, S. W.: Observed and simulated time evolution of HCl, $ClONO_2$, and HF total column abundances, Atmos. Chem. Phys., 12, 3527–3556, doi:10.5194/acp-12-3527-2012, 2012. 658

Kurylo, M. J. and Zander, R.: The NDSC–Its status after 10 yr of operation, in: Proceedings of XIX Quarennial Ozone Symposium, Hokkaido University, Sapporo, Japan, 167–168, 2000. 637

Lowe, D. C., Manning, M. R., Brailsford, G. W., and Bromley, A. M.: The 1991–1992 atmospheric methane anomaly: Southern Hemisphere 13C decrease and growth rate fluctuations, Geophys. Res. Lett., 24, 857–860, 1997. 660

Morgenstern, O., Zeng, G., Wood, S. W., Robinson, J., Smale, D., Paton-Walsh, C., Jones, N. B., and Griffith, D. W. T.: Long-range correlations in Fourier transform infrared, satellite, and modeled CO in the Southern Hemisphere, J. Geophys. Res., 117, D11301 doi:10.1029/2012JD017639, 2012. 659

Notholt, J. and Lehmann, R.: The moon as light source for atmospheric trace gas observations: measurement technique and analysis method, J. Quant. Spectrosc. Ra., 76, 435–445, 2003. 638

Notholt, J., Neuber, R., Schrems, O., and v. Clarmann, T.: Stratospheric trace gas concentrations in the Arctic polar night derived by FTIR-spectroscopy with the moon as IR light source, Geophys. Res. Lett., 20, 2059–2062, 1993. 638

Notholt, J., Meier, A., and Peil, S.: Total column densities of tropospheric and stratospheric trace gases in the undisturbed Arctic summer atmosphere, J. Atmos. Chem., 20, 311–332, 1995. 656

Olsen, S. C. and Randerson, J. T.: Differences between surface and column atmospheric CO_2 and implications for carbon cycle research, J. Geophys. Res., 109, D02301, doi:10.1029/2003JD003968, 2004. 636

Rinsland, C. P., Goldman, A., Elkins, J. W., Chiou, L. S., Hannigan, J. W., Wood, S. W., Mahieu, E., and Zander, R.: Long-term trend of at northern mid-latitudes: comparison between ground-based infrared solar and surface sampling measurements, J. Quant. Spectrosc. Ra., 97, 457–466, 2005. 637

Rodgers, C.: Inverse Methods for Atmospheric Sounding: Theory and Praxis, World Scientific Publishing Co., Singapore, 2000. 641, 642

Rothman, L. S, Jacquemart, D., Barbe, A., Benner, D. C., Birk, M., Brown, L. R, Carleer, M. R., Chackerian Jr., C., Chance, K., Coudert, L. H., Dana, V., Devi, V. M., Flaud, J.-M.,

AMTD
7, 633–701, 2014

Gamache, R. R., Goldman, A., Hartmann, J.-M., Jucks, K. W., Maki, A. G., Mandin, J.-Y., Massie, S. T., Orphal, J., Perrin, A., Rinsland, C. P., Smith, M. A. H., Tennyson, J., Tolchenov, R. N., Toth, R. A., Auwera, J. V., Varanasi, P., and Wagner, G.: The HITRAN 2004 molecular spectroscopic database, J. Quant. Spectrosc. Ra., 96, 139–204, 2005. 645

Rothman, L. S., Gordon, I. E., Barbe, A., Benner, D. C., Bernath, P. F., Birk, M., Boudon, V., Brown, L. R., Campargue, A., Champion, J.-P., Chance, K., Coudert, L. H., Dana, V., Devi, V. M., Fally, S., Flaud, J.-M., Gamache, R. R., Goldmanm, A., Jacquemart, D., Kleiner, I., Lacome, N., Lafferty, W., Mandin, J.-Y., Massie, S. T., Mikhailenko, S. N., Miller, C. E., Moazzen-Ahmadi, N., Naumenko, O. V., Nikitin, A. V., Orphal, J., Perevalov, V. I., A. Perrin, A. P.-C., Rinsland, C. P., Rotger, M., Šimečková, M., Smith, M. A. H., Sung, K., Tashkun, S. A., Tennyson, J., Toth, R. A., Vandaele, A. C., and Auwera, J. V.: The HITRAN 2008 molecular spectroscopic database, J. Quant. Spectrosc. Ra., 110, 533–572, 2009. 641

Schneider, M. and Hase, F.: Technical Note: recipe for monitoring of total ozone with a precision of around 1 DU applying mid-infrared solar absorption spectra, Atmos. Chem. Phys., 8, 63–71, doi:10.5194/acp-8-63-2008, 2008. 645

Schneider, M. and Hase, F.: Improving spectroscopic line parameters by means of atmospheric spectra: theory and example for water vapour and solar absorption spectra, J. Quant. Spectrosc. Ra., 110, 1825–1839, 2009. 639

Schneider, M., Hase, F., and Blumenstock, T.: Water vapour profiles by ground-based FTIR spectroscopy: study for an optimised retrieval and its validation, Atmos. Chem. Phys., 6, 811–830, doi:10.5194/acp-6-811-2006, 2006a. 639, 641

Schneider, M., Hase, F., and Blumenstock, T.: Ground-based remote sensing of HDO/H_2O ratio profiles: introduction and validation of an innovative retrieval approach, Atmos. Chem. Phys., 6, 4705–4722, doi:10.5194/acp-6-4705-2006, 2006b. 639, 641

Schneider, M., Barthlott, S., Hase, F., González, Y., Yoshimura, K., García, O. E., Sepúlveda, E., Gomez-Pelaez, A., Gisi, M., Kohlhepp, R., Dohe, S., Blumenstock, T., Wiegele, A., Christner, E., Strong, K., Weaver, D., Palm, M., Deutscher, N. M., Warneke, T., Notholt, J., Lejeune, B., Demoulin, P., Jones, N., Griffith, D. W. T., Smale, D., and Robinson, J.: Ground-based remote sensing of tropospheric water vapour isotopologues within the project MUSICA, Atmos. Meas. Tech., 5, 3007–3027, doi:10.5194/amt-5-3007-2012, 2012. 639

Sepúlveda, E., Schneider, M., Hase, F., García, O. E., Gomez-Pelaez, A., Dohe, S., Blumenstock, T., and Guerra, J. C.: Long-term validation of tropospheric column-averaged CH_4 mole

AMTD
7, 633–701, 2014

fractions obtained by mid-infrared ground-based FTIR spectrometry, Atmos. Meas. Tech., 5, 1425–1441, doi:10.5194/amt-5-1425-2012, 2012. 636, 637, 639, 641, 642, 652, 661, 665

Stiller, G., von Clarmann, T., Wegner, A., Baumann, M., Frank, E., and Oelhaf, H.: Retrieval of tropospheric versus stratospheric partitioning of HCl from ground-based MIPAS FTIR spectra, J. Quant. Spectrosc. Ra., 54, 899–912, 1995. 648

Sussmann, R., Forster, F., Rettinger, M., and Bousquet, P.: Renewed methane increase for five years (2007–2011) observed by solar FTIR spectrometry, Atmos. Chem. Phys., 12, 4885–4891, doi:10.5194/acp-12-4885-2012, 2012. 639

Velazco, V., Wood, S. W., Sinnhuber, M., Kramer, I., Jones, N. B., Kasai, Y., Notholt, J., Warneke, T., Blumenstock, T., Hase, F., Murcray, F. J., and Schrems, O.: Annual variation of strato-mesospheric carbon monoxide measured by ground-based Fourier transform infrared spectrometry, Atmos. Chem. Phys., 7, 1305–1312, doi:10.5194/acp-7-1305-2007, 2007. 657

Winderlich, J., Chen, H., Gerbig, C., Seifert, T., Kolle, O., Lavrič, J. V., Kaiser, C., Höfer, A., and Heimann, M.: Continuous low-maintenance CO_2/CH_4/H_2O measurements at the Zotino Tall Tower Observatory (ZOTTO) in Central Siberia, Atmos. Meas. Tech., 3, 1113–1128, doi:10.5194/amt-3-1113-2010, 2010. 651

WMO: Brailsford, G. (Ed.), Report of the 16th WMO/IAEA Meeting on Carbon Dioxide, Other Greenhouse Gases, and Related Measurement Techniques (GGMT-2011), GAW Report No. 206, Wellington, New Zealand, 2012. 669

Wood, S. W., Bodeker, G. E., Boyd, I. S., Jones, N. B., Connor, B. J., Johnston, P. V., Matthews, W. A., Nichol, S. E., Murcray, F. J., Nakajima, H., and Sasano, Y.: Validation of version 5.20 ILAS HNO_3, CH_4, N_2O, O_3, and NO_2 using ground-based measurements at Arrival Heights and Kiruna, J. Geophys. Res., 107, D24, ILS 5-1–ILS 5-11, doi:10.1029/2001JD0005812002, 2002. 660

Wood, S. W., Batchelor, R. L., Goldman, A., Rinsland, C. P., Connor, B. J., Murcray, F. J., Stephen, T. M., and Heuff, D. N.: Ground-based nitric acid measurements at Arrival Heights, Antarctica, using solar and lunar Fourier transform infrared observations, J. Geophys. Res.-Atmos., 109, D18, doi10.1029/2004JD004665, 2004. 638

Wunch, D., Toon, G. C., Wennberg, P. O., Wofsy, S. C., Stephens, B. B., Fischer, M. L., Uchino, O., Abshire, J. B., Bernath, P., Biraud, S. C., Blavier, J.-F. L., Boone, C., Bowman, K. P., Browell, E. V., Campos, T., Connor, B. J., Daube, B. C., Deutscher, N. M., Diao, M., Elkins, J. W., Gerbig, C., Gottlieb, E., Griffith, D. W. T., Hurst, D. F., Jiménez, R., Keppel-Aleks, G., Kort, E. A., Macatangay, R., Machida, T., Matsueda, H., Moore, F., Morino, I.,

AMTD
7, 633–701, 2014

Park, S., Robinson, J., Roehl, C. M., Sawa, Y., Sherlock, V., Sweeney, C., Tanaka, T., and Zondlo, M. A.: Calibration of the Total Carbon Column Observing Network using aircraft profile data, Atmos. Meas. Tech., 3, 1351–1362, doi:10.5194/amt-3-1351-2010, 2010. 665

Zellweger, C., Steinbacher, M., Buchmann, B., and Scheel, H. E.: System and Performance Audit of Surface Ozone, Methane, Carbon Dioxide, Nitrous Oxide and Carbon Monoxide at the Global GAW Station Lauder, New Zealand, March 2010, WCC-Empa Report 10/3, available at: http://gaw.empa.ch/audits/LAU_2010.pdf (last access: 10 December 2013), 2010. 670

AMTD
7, 633–701, 2014

Table 1. Ground-based NDACC FTIR contributing sites.

Site (acronym)	Location	Altitude a.s.l. [m]	Instrument	Contributor
Eureka, EU	80.1° N, 86.4° W	610	125HR	University of Toronto
Ny-Ålesund, NA	78.9° N, 11.9° W	15	120HR	University of Bremen and Alfred Wegener Institute
Kiruna, KI	67.8° N, 20.4° E	419	120/5HR	Karlsruhe Inst. of Tech. and Inst. for Space Phys. Kiruna
Bremen, Br	53.1° N, 8.9° E	27	125HR	University of Bremen
Karlsruhe, KA	49.1° N, 8.9° E	111	125HR	Karlsruhe Inst. of Tech.
Izaña, IZ	28.3° N, 16.5° E	2367	120/5HR	Karlsruhe Inst. of Tech. and Meteorological State Agency of Spain
Wollongong, WO	34.4° S, 150.9° E	30	125HR	University of Wollongong
Lauder, LA	45.1° S, 169.7° E	370	120HR	National Institute of Water and Atmospheric Research
Arrival Heights, AH	77.8° S, 166.7° E	250	120M	National Institute of Water and Atmospheric Research and University of Denver

AMTD
7, 633–701, 2014

Table 2. Uncertainty sources used for our error estimation. The third column gives the uncertainty value and the fourth column the partitioning of this uncertainty between statistical and systematic sources.

Error source	Acronym	Uncertainty	Statistical/ Systematic
Measurement Noise	noi	0.4 %	100/0
Baseline (Channeling and Offset)	bas	0.1 % and 0.1 %	50/50
Mod. Eff. and Pha. Err.	ils	10 % and 0.1 rad	50/50
Temperature Profile	tem	2–5 K	70/30
Line Of Sight	los	1°	90/10
Solar Lines (Intensity and ν-scale)	sol	1 % and 10^{-6}	80/20
Humidity Profile	hum	10 % (2 km corr. length)	50/50
Spectroscopic Parameters (S and γ)	spe	2 %	0/100

AMTD
7, 633–701, 2014

Table 3. Typical DOFS for the CH_4 FTIR retrievals and typical smoothing errors (root-square-sum of bl, tro, and utls), total statistical errors, and total systematic errors for the lower tropospheric column-averaged CH_4 amounts. The error values are calculated according to the assumed uncertainty and statistical/systematic partitions as given in Table 2 and are for the a posteriori corrected retrievals as described in Sect. 2.3.3. The error values obtained without the a posteriori correction are given in parentheses.

Station	DOFS	Smoothing [%]	Statistical [%]	Systematic [%]
Eureka, EU	2.51	0.83 (1.52)	0.91 (0.92)	2.56 (2.58)
Ny-Ålesund, NA	2.27	0.95 (1.75)	0.69 (0.70)	2.29 (2.27)
Kiruna, KI	2.61	0.82 (1.51)	0.98 (1.00)	2.59 (2.60)
Bremen, BR	2.48	0.91 (1.40)	0.86 (0.88)	2.42 (2.40)
Karlsruhe, KA	2.57	0.93 (1.39)	1.07 (1.10)	2.54 (2.52)
Izaña, IZ	2.51	0.84 (1.14)	1.28 (1.29)	2.53 (2.51)
Wollongong, WO	2.60	0.97 (1.15)	1.06 (1.06)	2.53 (2.52)
Lauder, LA	2.52	0.93 (1.22)	1.21 (1.22)	2.66 (2.65)
Arrival Heights, AH	2.14	1.10 (2.23)	0.70 (0.72)	2.34 (2.30)

AMTD
7, 633–701, 2014

Table 4. In-situ surface contributing sites. Instrument acronym: GC, Gas Chromatography; FID, Flame Ionization Detection; CRDS, Cavity Ringdown Spectroscopy. Interval time means the time frequency of the data available used in this study.

Site, acronym	Location	Altitude a.s.l. [m]	Measurement method	Sampling type	Interval time	Contributor (acronym)
Alert, AL	82.45° N, 62.52° W	210	GC-FID	Continuous	hourly	Environment Canada (EC)
Ny-Ålesund, NA	78.90° N, 11.88° E	475	GC-FID	Flasks	monthly	Earth System Research Laboratory, NOAA (NOAA/ESRL)
Pallas-Sammaltunturi, PS	67.97° N, 24.12° E	560	GC-FID: 2004–2008; CRDS: since 2009	Continuous	hourly	Finnish Meteorological Institute (FMI)
Mace Head, MH	53.33° N, 9.90° W	8	GC-FID	Continuous	monthly	Advanced Global Atmospheric Gases Experiment Science Team (AGAGE)
Schauinsland*, SC	47.92° N, 7.92° E	1205	GC-FID	Continuous	hourly	Federal Environmental Agency Germany (UBA)
Jungfraujoch, JU	46.55° N, 7.99° E	3580	GC-FID: 2005–2009; CRDS: since 2010	Continuous	hourly	Swiss Federal Laboratories for Materials Science and Technology (EMPA)
Izaña, IZ	28.30° N, 16.50° W	2367	GC-FID	Continuous	hourly	Izaña Atmospheric Research Center, Meteorological State Agency of Spain (AEMET)
Cape Ferguson*, CF	19.28° S, 147.05° E	2	GC-FID	Flasks	event	Commonwealth Scientific and Industrial Research Organisation (CSIRO)
Cape Grim, CG	40.68° S, 144.68° E	94	GC-FID	Continuous	event	Advanced Global Atmospheric Gases Experiment Science Team (AGAGE)
Lauder, LA	45.1° S, 169.7° E	370	in-situ FTIR	Continuous	hourly	National Institute of Water and Atmospheric Research (NIWA)
Arrival Height*, AH	77.80° S, 166.67° E	184	GC-FID	Flask	event	National Institute of Water and Atmospheric Research (NIWA)

* indicate a GAW regional site, the rest sites are global sites.

AMTD
7, 633–701, 2014

Table 5. NDACC FTIR vs. GAW tropospheric CH_4 data comparison: stations, time scales, filter applied for obtaining regional-scale GAW data, and number of coincidences.

NDACC site	GAW site	Time scale	Filter applied to GAW data	Coincidences
Eureka	Alert	monthly	standard deviation	33
Ny-Ålesund	Ny-Ålesund	monthly	no filter	22
Kiruna	Pallas-Sammaltunturi	monthly	standard deviation	51
Bremen	Mace Head	monthly	no filter	65
Karlsruhe	Schauinsland	daily	combination of stations	162
Izaña	Izaña	daily	night time	225
Wollongong	Cape Grim	monthly	combination of stations	36
Lauder	Lauder	monthly	time, wind $\geq 5\,m\,s^{-1}$, and standard deviation	47
Arrival Heights	Arrival Heights	monthly	standard deviation	21

AMTD
7, 633–701, 2014

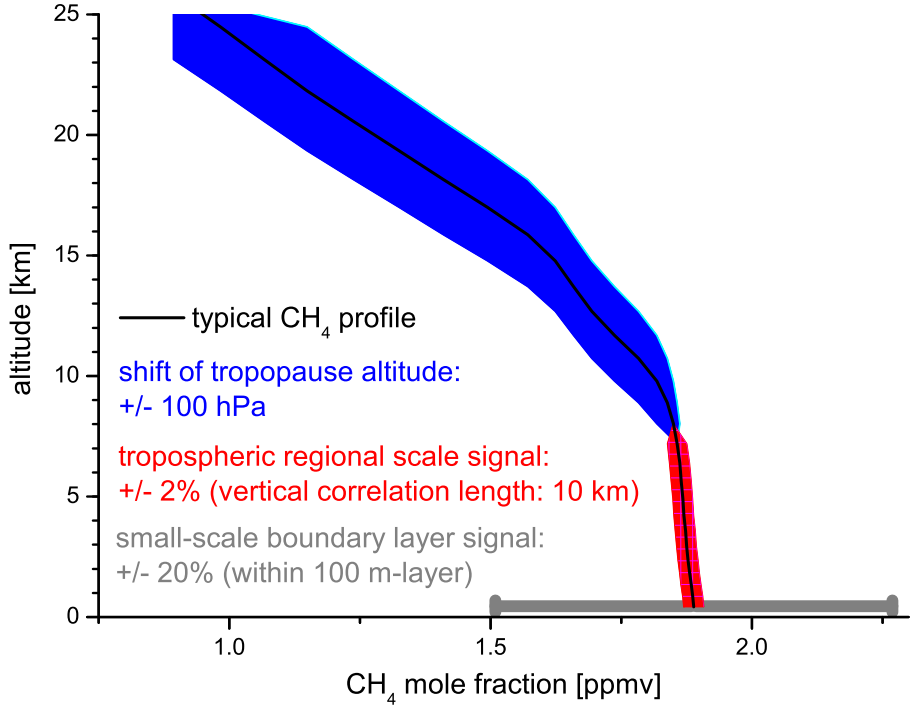

Fig. 1. Typical atmospheric CH_4 signals. Grey bar: near-surface boundary layer variability; red area: tropospheric regional-scale variability; blue area: UTLS variability caused by shifts in the tropopause altitude.

AMTD
7, 633–701, 2014

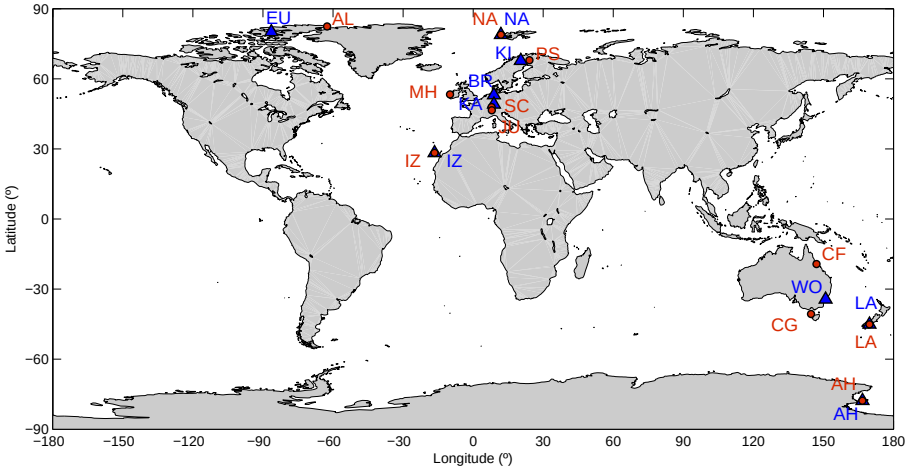

Fig. 2. NDACC FTIR stations in blue solid triangles and GAW in-situ stations in orange solid circles. See Tables 1 and 4 for the full station names.

AMTD
7, 633–701, 2014

NDACC FTIR and GAW surface in-situ tropospheric CH_4

E. Sepúlveda et al.

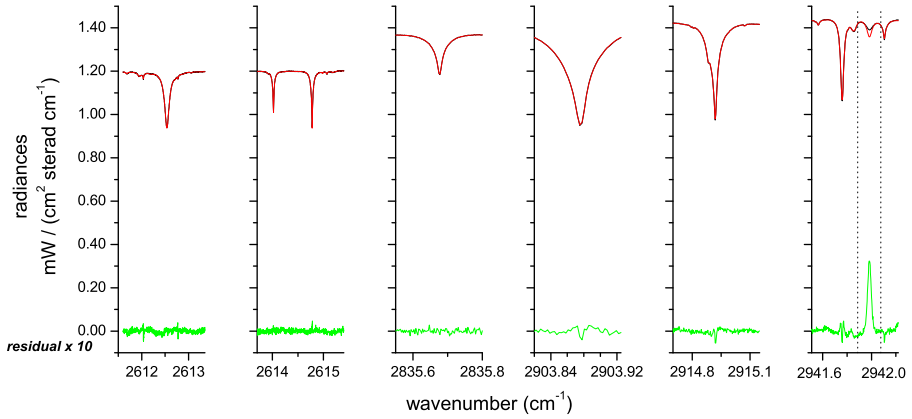

Fig. 3. Spectral microwindows applied to retrieve the tropospheric CH_4 mole fraction. It shows measured spectrum (black), simulated spectrum (red), and residuals multiplied by a factor of 10 (green). The black dashed lines in the last microwindow delimit an absorption line that is not included in the retrieval process.

AMTD
7, 633–701, 2014

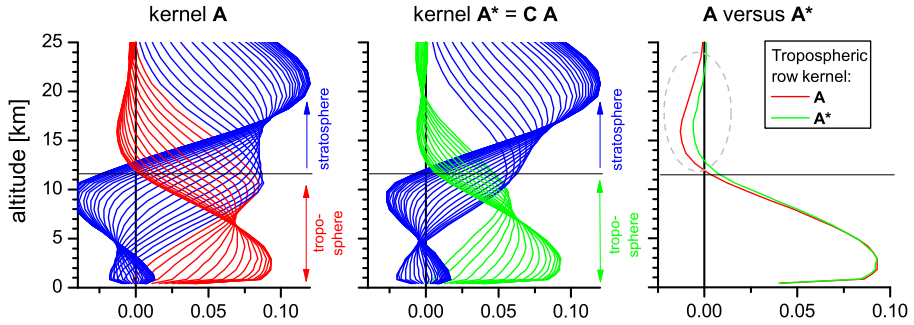

Fig. 4. Row averaging kernels of the CH_4 product for a typical observation at the subarctic site of Kiruna. Left panel: kernels $\hat{\mathbf{A}}$ obtained from the Tikhonov–Phillips profile retrieval (red: tropospheric kernels, blue: UTLS kernels). Central panel: kernels $\mathbf{A}^*$ obtained after applying the a posteriori optimisation of Eq. (11) (green: tropospheric kernels, blue: UTLS kernels). Right panel: comparison of the surface row kernels $\hat{\mathbf{A}}$ (red line) and $\mathbf{A}^*$ (green line). The typical altitude where the UTLS starts is indicated by the horizontal black line (11.5 km).

AMTD
7, 633–701, 2014

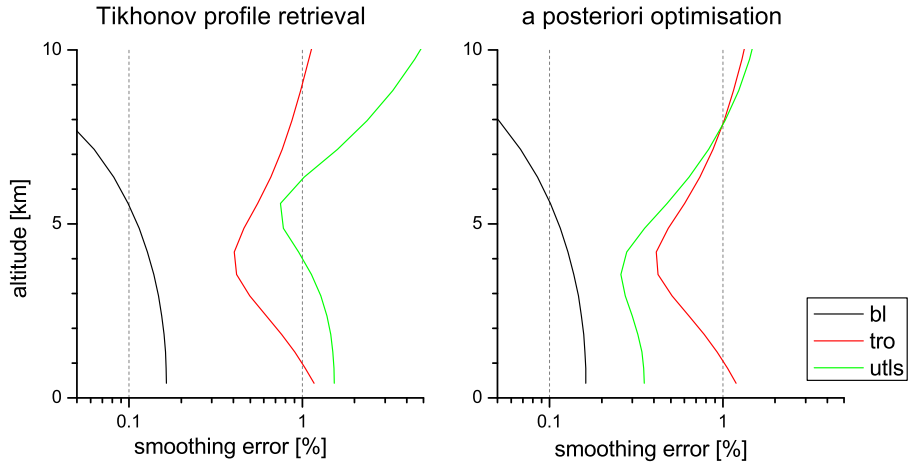

Fig. 5. Estimated smoothing errors for CH_4 for small-scale boundary layer variability (black line), tropospheric variability (red line), and variability in the UTLS due to a tropopause altitude shift (green line). Left panel: for the Tikhonov–Phillips profile retrieval. Right panel: after applying the a posteriori optimisation.

AMTD
7, 633–701, 2014

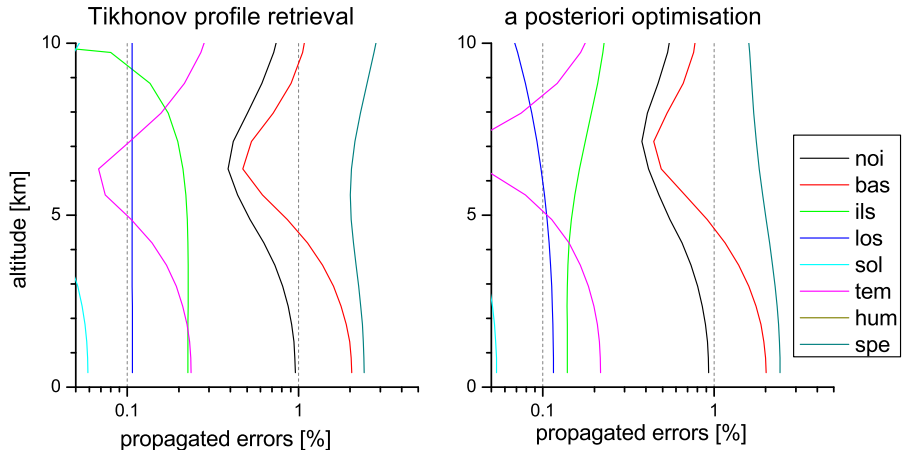

Fig. 6. Errors propagation for CH_4 due the uncertainties as listed in Table 2 in the third column. Error sources as given in the legend: noi (measurement noise), bas (baseline), ils (instrumental line shape), los (line of sight), sol (solar lines), tem (atmospheric temperature), hum (cross dependency on humidity; this error is smaller than 0.02 %), and spe (spectroscopic parameters). Left panel: for the Tikhonov–Phillips profile retrieval. Right panel: after applying the a posteriori optimisation.

AMTD
7, 633–701, 2014

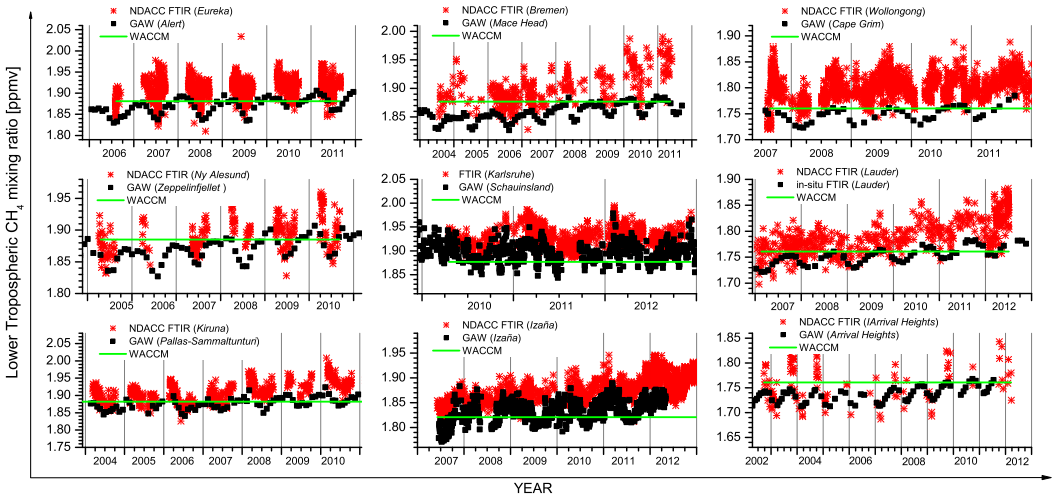

Fig. 7. Tropospheric column-averaged CH_4 mole fraction measured by NDACC FTIR (red stars) and GAW in-situ (black squares) at the nine different sites. Shown are all FTIR data and the GAW data that are representative for regional-scale signals (the filter methods are described in Sects. 3.2–3.10). These are daily data for Schauinsland and Izaña and monthly data for the rest of the GAW stations. The green line represents the WACCM apriori mole fraction applied for the NDACC FTIR retrievals.

AMTD
7, 633–701, 2014

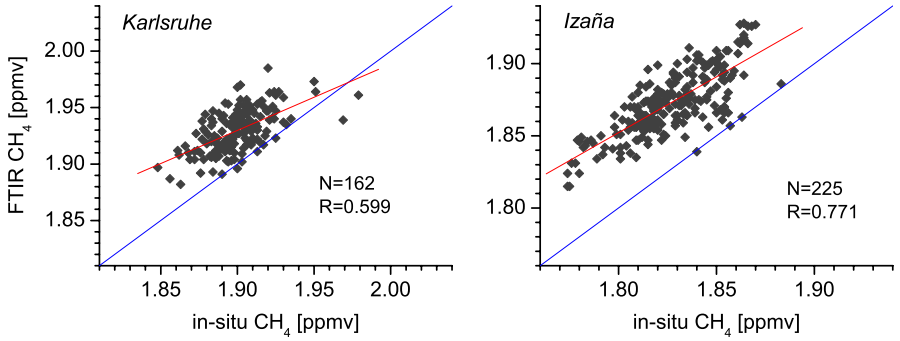

Fig. 8. Correlation plot between coincident tropospheric CH_4 daily medians obtained by NDACC FTIR and in-situ GAW for the Karlsruhe (left graph) and Izaña (right graph) FTIR sites. The blue lines indicate the 1 : 1 diagonal.

AMTD
7, 633–701, 2014

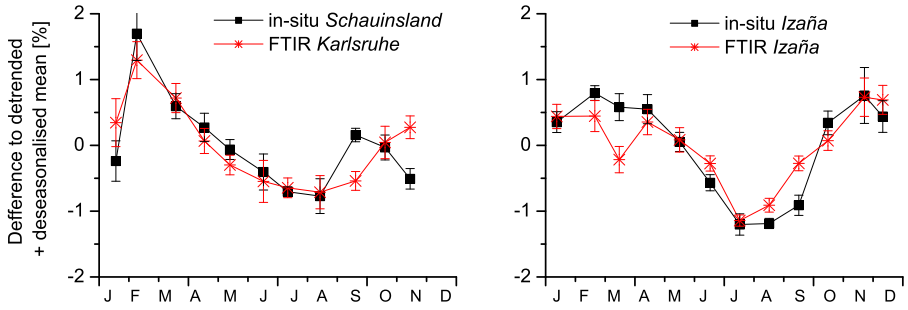

Fig. 9. Seasonal cycle for Karlsruhe (left graph) and Izaña (right graph) stations obtained by NDACC FTIR (red stars) and in-situ GAW CH_4 mole fraction (black squares), respectively.

AMTD
7, 633–701, 2014

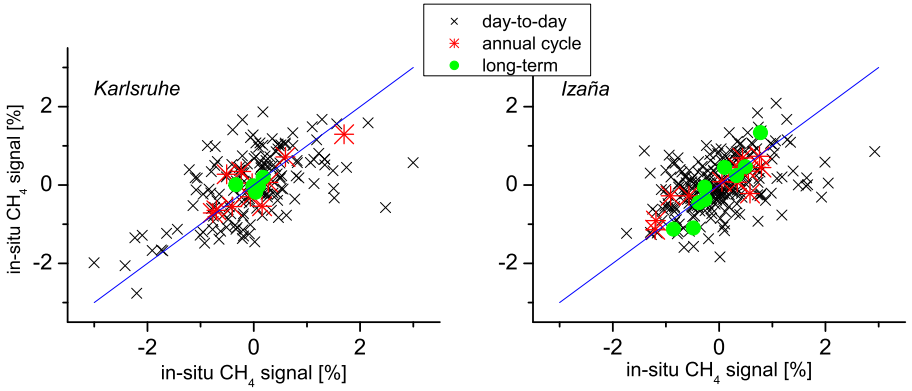

Fig. 10. NDACC FTIR/GAW correlation plots for CH_4 variations/signals on different time scales. Left graph: for Karlsruhe; right graph: for Izaña. The day-to-day variation is shown as black crosses, the monthly variation (annual/seasonal cycle) as red stars, and the long-term variation as green circles.

AMTD
7, 633–701, 2014

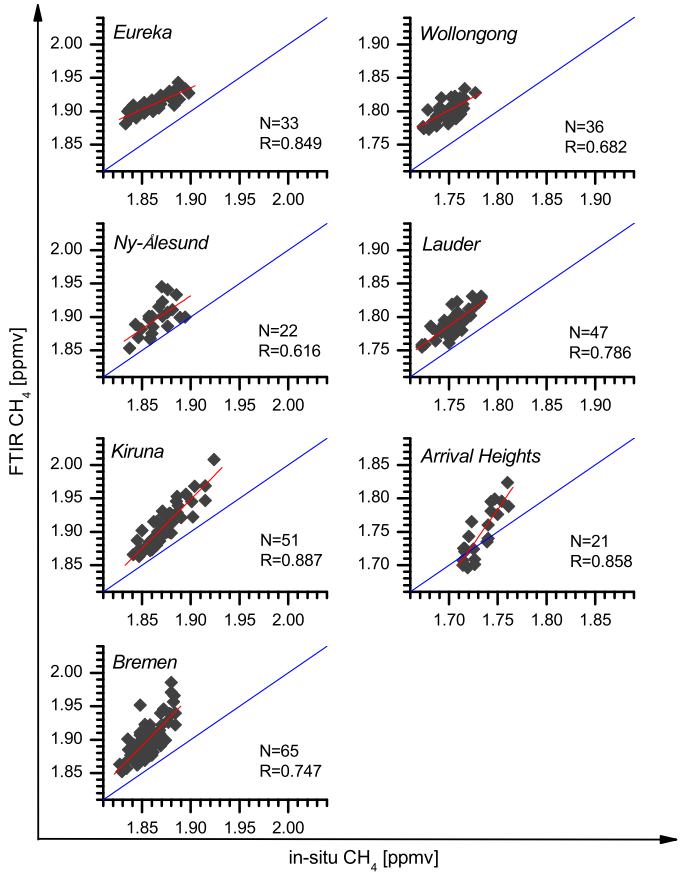

Fig. 11. Same as Fig. 8 but for the rest of the stations and for coincident data within ±15 days. The corresponding station name is shown in each graph.

AMTD
7, 633–701, 2014

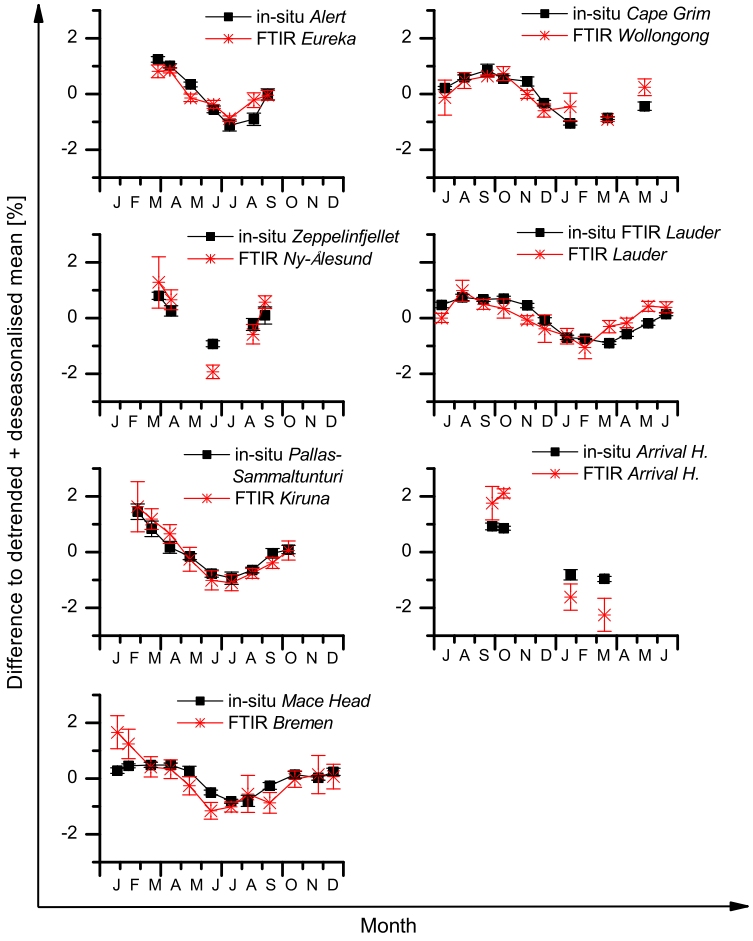

Fig. 12. Same as Fig. 9 but for the rest of the stations. The stations names are shown in each graph.

AMTD
7, 633–701, 2014

NDACC FTIR and GAW surface in-situ tropospheric CH_4

E. Sepúlveda et al.

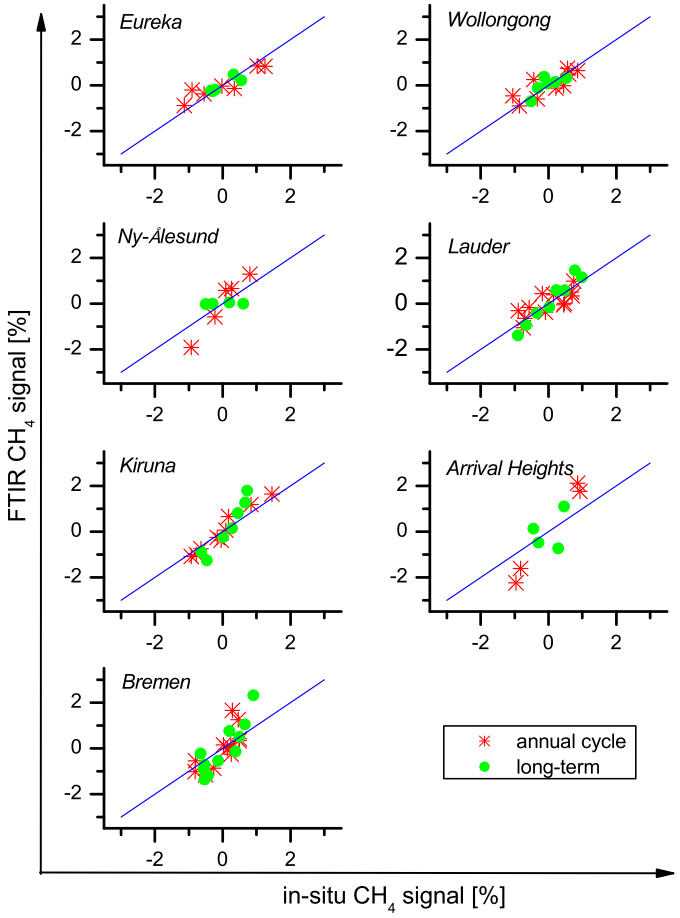

Fig. 13. Same as Fig. 10 but for the rest of the stations and only for the seasonal/annual cycle variability and the long-term variability.

AMTD
7, 633–701, 2014

NDACC FTIR and GAW surface in-situ tropospheric CH_4

E. Sepúlveda et al.

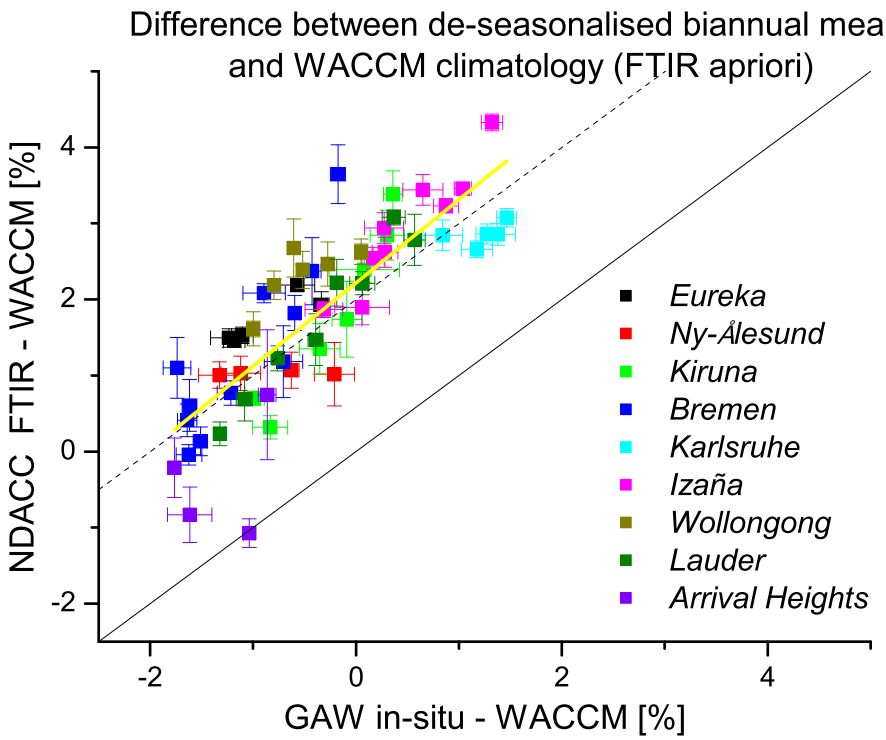

Fig. 14. Network consistency between GAW and NDACC FTIR. Plotted are the difference between the de-seasonalised biannual mean data and the WACCM climatology (FTIR apriori) for GAW and NDACC FTIR at the nine stations. The solid and dashed black lines indicate the 1 : 1 diagonal, being the dashed line + 2 % off. The solid yellow line shows the regression line.

AMTD
7, 633–701, 2014

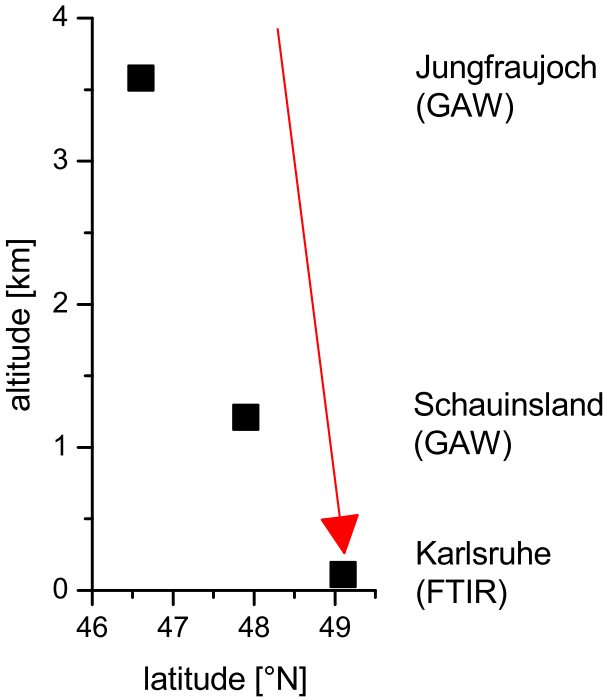

Fig. A1. Location of the Central European GAW stations and the Karlsruhe FTIR instrument. Red arrow is indicative for the line of sight of the FTIR instrument.

AMTD
7, 633–701, 2014

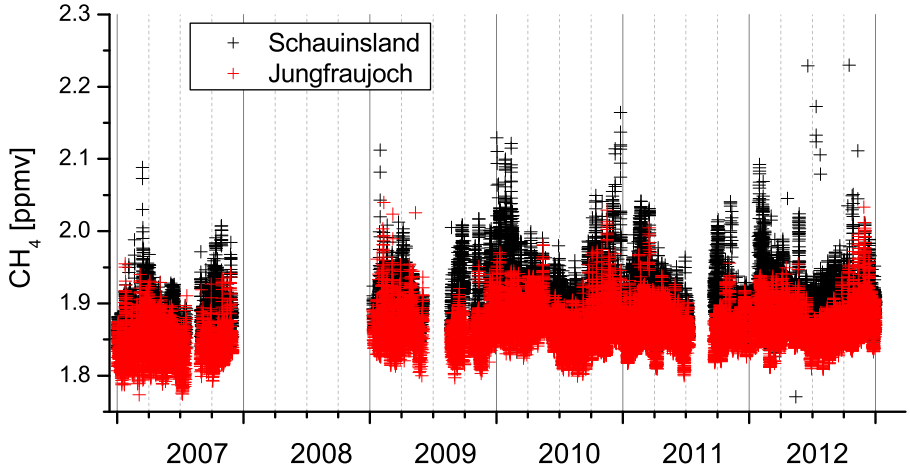

Fig. A2. Overview of the coincident Schauinsland and Jungfraujoch in-situ CH_4 time series.

AMTD
7, 633–701, 2014

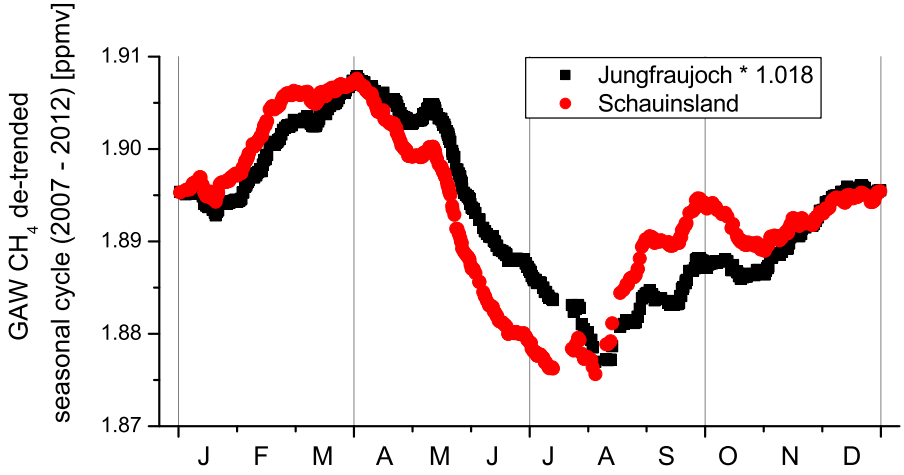

Fig. A3. De-trended seasonal cycles observed in the in-situ data of Schauinsland and Jungfraujoch. The Jungfraujoch CH_4 mole fraction are roughly 2 % lower than the Schauinsland mole fraction.

AMTD
7, 633–701, 2014

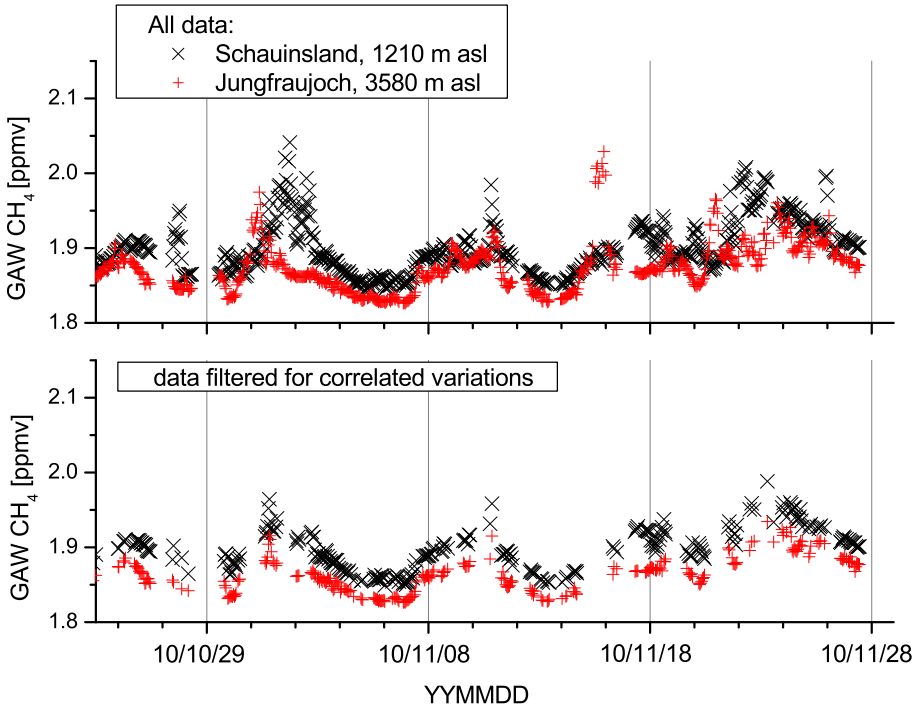

Fig. A4. Example of Schauinsland and Jungfraujoch CH_4 in-situ data for a period in November 2010. Upper panel: all data. Lower panel: data retained after applying the filter for common signals.

AMTD
7, 633–701, 2014

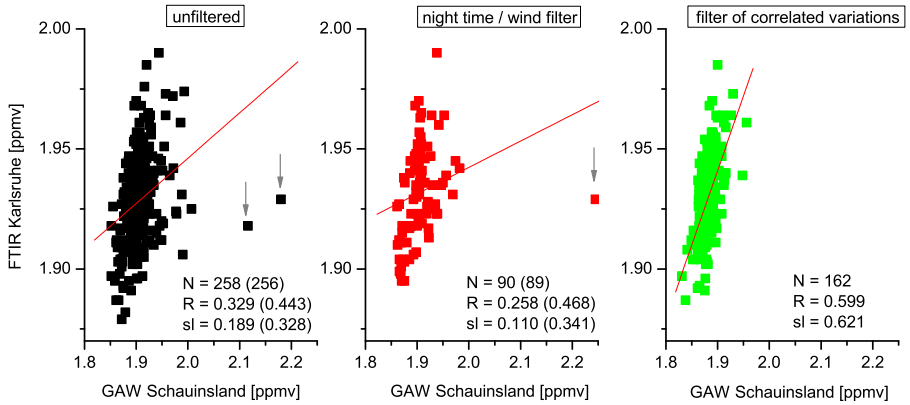

Fig. A5. Comparison of coincident Schauinsland in-situ and Karlsruhe FTIR CH_4 data for different in-situ data filters. Left panel: unfiltered data; central panel: nighttime/wind filter; right panel: filter for common signals in the Jungfraujoch and Schauinsland data. The regression lines are shown as red line. The number of achieved daily coincidences (N), the correlation coefficient (R), and the slope of the regression line (sl) is written in each graph. The N, R, and sl values after removing outliers (which are marked by arrows) are given in parentheses. Please note that the plot on the right panel is also shown in Fig. 8 (left panel) but there on an optimised scale.

AMTD
7, 633–701, 2014